

Review

# Recent Developments on the Synthesis of Nanocomposite Materials via Ball Milling Approach for Energy Storage Applications

Josny Joy <sup>1</sup>, Anand Krishnamoorthy <sup>2</sup>, Ashish Tanna <sup>3</sup>, Vishal Kamathe <sup>4</sup>, Rupali Nagar <sup>4</sup>  
and Sessa Srinivasan <sup>5,\*</sup>

<sup>1</sup> Center for Advanced 2D Materials, National University of Singapore, 6 Science Drive 2, Singapore 117546, Singapore

<sup>2</sup> Apcotex Industries Limited, MIDC Industrial Area, Taloja, Navi Mumbai 410208, Maharashtra, India

<sup>3</sup> Department of Physics, School of Sciences, RK University, Rajkot 360020, Gujarat, India

<sup>4</sup> Nanomaterials for Energy Applications Lab, Applied Science Department, Symbiosis Institute of Technology, Symbiosis International (Deemed University), Lavale, Pune 412115, Maharashtra, India

<sup>5</sup> Department of Engineering Physics, Florida Polytechnic University, Lakeland, FL 33805, USA

\* Correspondence: ssrinivasan@floridapoly.edu; Tel.: +1-8134511876

**Featured Application:** The focus of this research paper is to deploy ball milled nanocomposite materials for potential energy storage applications.

**Abstract:** This review is focused on the topical developments in the synthesis of nanocomposites using the simplest top-down approach, mechanochemical milling, and the related aspects of the interfacial interactions. Milling constraints include time duration of milling, ball size, the ball-to-sample content proportion, rotation speed, and energy that took part in a vital part of the structure–property relationships and composite interactions. Milled nanocomposites are being used in different structural applications for their higher performance rate and throughput. The synthesis of different nanocomposites and the effect of various parameters on the mill-ability of nanocomposites are discussed. Moreover, some of the major advancements in the energy sector are discussed in the latter part of the review.

**Keywords:** ball milling; nanocomposites; mechanochemistry; energy storage; alloying



**Citation:** Joy, J.; Krishnamoorthy, A.; Tanna, A.; Kamathe, V.; Nagar, R.; Srinivasan, S. Recent Developments on the Synthesis of Nanocomposite Materials via Ball Milling Approach for Energy Storage Applications. *Appl. Sci.* **2022**, *12*, 9312. <https://doi.org/10.3390/app12189312>

Academic Editors: Young-Kyu Han, Sessa S. Srinivasan and Vërsha Khare

Received: 27 July 2022

Accepted: 13 September 2022

Published: 16 September 2022

**Publisher's Note:** MDPI stays neutral with regard to jurisdictional claims in published maps and institutional affiliations.



**Copyright:** © 2022 by the authors. Licensee MDPI, Basel, Switzerland. This article is an open access article distributed under the terms and conditions of the Creative Commons Attribution (CC BY) license (<https://creativecommons.org/licenses/by/4.0/>).

## 1. Introduction

The first ever produced dispersion-strengthened alloys with distribution of uniform dispersoid were synthesized by the powder metallurgy method commonly known as mechanochemical alloying [1]. It is further used as a powerful non-equilibrium processing method that can be deployed to synthesize a variety of meta-stable structured materials [2]. Categorically, the milling of particles is classified as (i) mechanical milling where the similar nature of elements or compounds can be milled, and (ii) mechanical alloying where dissimilar constituents can be milled with transfer or sharing of material species [2–4]. The advent of ball milling thus supported the production of nanostructure materials that are meta-stable when compared to their pristine counterparts. The grain size refinement is a controllable property based on the mechanochemical agitation, features, and properties of the constituent powders involved in the milling technique and, finally, the amounts of defects and/or dislocations introduced based on the plastic deformation during the thermal recovery processes [2].

In a typical high energy mechanochemical milling process, the reactive ingredients are added with the required balls and the media in a closed container. Then, after specific milling experiment, very fine particulates of the product are obtained, which are often of micrometric size; however, the components that are welded together are nano-sized,

for industrial and research quality. The “media” refers to fluids (for example, liquid media such as solvents, DI, surfactants, or dispersants, and gaseous media such as air, argon, nitrogen, and reactive atmospheres, namely, hydrogen). The root cause of nanostructural formation could be due to the two concurrent processes, particle fracturing and agglomeration/aggregation (or cold welding in the case of mechanical alloying) that occur at different rates. Additionally, the milled product exhibits a large number of defect accumulation sites. Compared to many other synthesis techniques, solid state milling has dual advantages, for example, this process can not only produce ultra-fine nanoparticles with definite stoichiometric ratios, but also enable those products with high yield, greater densification, and homogeneity. However, a segregation phenomenon like presence of reagents residue that is unavoidable during the milling of diverse materials [3]. For the development of new and advanced materials, with appropriate stress–strain characteristics, the ball milling or rod milling techniques have been considered potential and powerful tools. The mechanical alloying is a unique technique that can be performed at ambient conditions and with different types of mills, such as high (or low) energy, centrifugal type, attritor type, vibratory type, and tumbling type.

In the vibratory type of ball mill, grinding of the materials can be performed with vibratory motions with high frequencies and low amplitudes. The ball’s velocity in the vibratory milling apparatus is much greater than that of planetary ball mill system; therefore, less time may be needed for the particle size reduction in the vibratory ball mills. Here, the similar parameters need to be considered at time of milling process, i.e., milling speed, milling time, grinding medium, atmosphere, etc. Another type of milling apparatus involving planetary motions of the sample vials containing the materials to be grinded are called planetary ball mills. In this planetary milling method, an equal magnitude, as well as an opposite direction of forces with the containers and the underneath support disks, often produces both friction (due to balls rolling on the walls) and severe impact (due to the balls hits each other or with the milled powder). In a single event of planetary ball mill, at least few hundred grams of the initial powders can be milled with high consistency and uniformity. Greater control of rotation speed of individual containers with respect to the support surfaces have recently been developed in modern instruments by different manufacturers [4–6]. In both the laboratory scale and an industrial scale ball milling, an important physical parameter, such as kinetic energy ( $K.E. = \frac{1}{2} mv^2$ ) of the energetic balls having a specific mass moving with the agitation velocity, contributes and determines the effectiveness and the total duration required in addition to particle size reduction. Therefore, based on the kinetic energy value in a laboratory scale apparatus, the vibratory mill, due to the higher velocity, induces faster transformation while the ball mass is kept constant when compared to the planetary ball mill. However, an industrial scale vibratory mill, due the containment of velocity, leads slower transformation with respect to other types of mills.

The mechanochemical alloying is considered as the versatile method for the manufacture of oxide composites in large quantities [7]. The uniqueness of this alloying process is due to the high energy induced repeated collisions of the constituents, fracturing, and cold welding of the candidate materials, such as amorphous and/or nanostructure materials [8]. Another competing characteristic of the ball milling processes is that the scaling of materials’ manufacturing to industrial quantities are not cumbersome. The mechanochemical milling not only influences the attrition and agglomeration behavior of the materials involved, but also induces the chemical reactivity that eventually decides the final product and its properties. With this advantage of additional features of mechanical alloying induced chemical transformation reactions, a number of metal oxide nanocomposites have been milled with more reactive materials. Therefore, utilizing mechanochemical processes in place of mechanical alloying has a difference when we deal with the reactive chemical species that yields a desired product [9].

A typical ball mill can be constructed with a hollow cylindrical chamber that is made to rotate about a horizontal axis and is filled with different dimension balls. Depending on

the characteristics of the materials to be milled, different material types of the container and the balls are chosen, for example, stainless steel, tungsten carbide, zirconia, alumina, agate, or silicon nitride. In order to avoid a reaction with the container walls, these are coated with liner based on manganese, steel, or rubber material. In the category of reactive mechanochemical milling, a low vacuum ( $\sim 10^{-3}$  Torr), or special purpose gases, such as argon, hydrogen, nitrogen, will be deployed while the milling process is underway. Many of the ball mill types, such as attrition, planetary, vibratory, and low-energy tumbling, are often handling variable temperatures and pressures which are convenient for in-situ processing and optimization [10]. The mechanochemical pulverization process breaks the chemical bonds through the energy of the kinetic motions of the impacted balls, which crush the bulk material to give small particles and generate new surfaces and properties. In 2020, Tanna et al. prepared and studied the effect of multiferroic composite materials which are free from the lead metal and are synthesized via the high energy mechanical alloying techniques [11].

The ball milling technique is a versatile top-down synthesis technique to synthesize nanomaterials, including metallic, multi-metallic, alloyed, ceramic nanocomposites, etc. It is a simple, economical, and high throughput top-down fabrication method for nanocomposites compared to other techniques. Ball milling reinforces the particles onto the surface or into the interlayers of the matrix phase of the composite [12]. This could be performed with/without solid-state chemical reaction. The mechanochemical milling process includes the synthesis of various nanocomposite materials such as metal matrix [13–20], polymer matrix [21], and ceramic matrix [22,23] nanocomposites.

Metallic particles and reinforcing particles (nanomaterials) are mixed and ground in a sample jar containing a large number of balls. Progressive, repeated collisions between the particles, balls, and vessel walls leads to particle fracturing and cold-welding mechanism where compression, shear, and frictional forces act together to break down the material into nano-powder. These mechanisms result in the formation of the fine metallic nanocomposite powder corresponding to the initial state. The advantage of mechanochemical alloying is the homogenous distribution of compounded particles into the matrix, which prevent agglomeration. During the milling process, the matrix phase is deformed plastically while the compounding particulates become finer due to persistence of ball and powder collisions. The metal may become flattened and is then welded together and the fragmented reinforcing material is embedded together between two or more metallic particles. The properties of ball milled nanocomposites are mainly affected by matrix strength, dispersion of nanofiller, porosity, active surface area, interfacial interactions, and reactions. The interfacial bonding influences the properties of the nanocomposites. An efficient bonding could be established by modifying the wettability angle at the interface. This is usually achieved via the sintering process [24]. The process is depicted in Figure 1 where the particles inserted onto the interfacial boundaries of the welded metal have been shown explicitly.

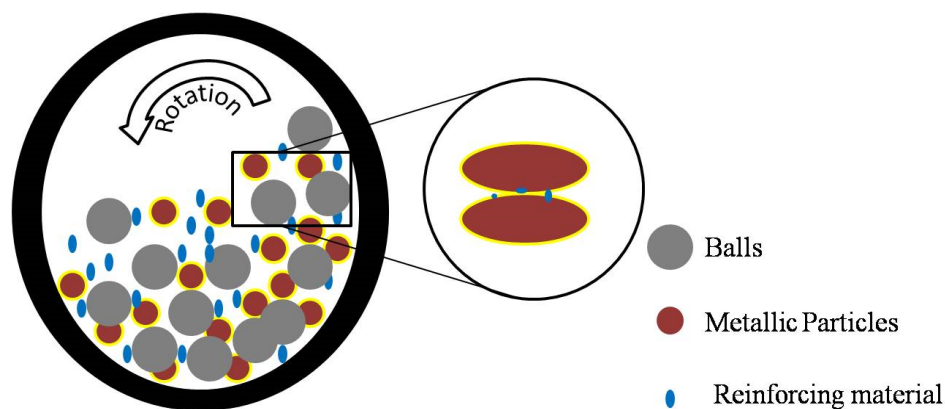


**Figure 1.** Schematic of metallic nanocomposite ball milling process. Inserted: the particle embedded onto the interfacial boundaries of the metallic matrix after mechanical alloying.

The most common method for the preparation of polymer nanocomposite via top-down approach is the wet milling method. The polymer and the filler are dispersed in a solvent medium. The size of the filler gets reduced and simultaneous polymerization occurs when subjected to mechanical agitation. These alloyed particles tend to agglomerate or recrystallize to maintain minimum Gibbs free energy. Process control agents or solvents are used to prevent aggregation and to maintain stability. High energy ball milling exerts higher kinetic energy ( $\sim 30$  mJ) refers the impact of a single ball collision that is traveling with a velocity of at least 3.6 m/s. than the conventional ball milling ( $\sim 5$  mJ) [25]. Faster phase transformation and particle size reduction can be achieved at a minimum milling time with high energy mechanical milling process [26]. Optimizing the parameters for the milling process tends to have a great effect on obtaining a stable homogeneous dispersion of particles [27]. The preparation of polymer nanocomposites via the top-down method is discussed in relation to metallic nanocomposite synthesis.

## 2. Type of Ball Mills

### 2.1. Based on Mechanical Energy

Mechano-chemical milling can be categorized based on the mechanical energy induced onto the sample inside the chamber as low (LEBM) and high energy ball mills (HEBM). The energy released via collision and attrition between the balls and the samples directly impacts the formation of nanomaterials with high specific surface area [28]. Wei X. et al. have prepared biochar/copper oxide (BC/CuO) nanocomposite with a surface area of  $330.0 \text{ m}^2 \text{ g}^{-1}$  where the size of CuO is 10.4 nm using HEBM [29]. Horizontal mills fall under the LEBM, while HEBM includes planetary, attrition, and vibratory mills (Figure 2).

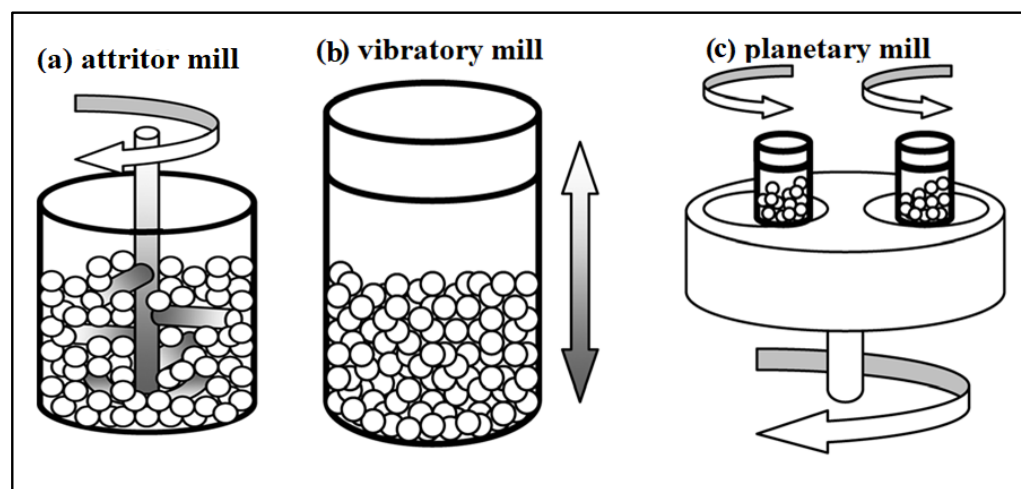


**Figure 2.** Schematic representation of various types of ball mills [30] “Reprinted/adapted with permission from Ref. [30]. 1999, Royal Society of Chemistry (Great Britain)”. More details on “Copyright and Licensing are available via the following link: <http://creativecommons.org/licenses/by/4.0/> (accessed on 29 August 2022).

### 2.2. Based on Operation Mode

Direct and indirect milling are the two modes, depending on their operations. In the former, kinetic energy (KE) is directly imparted onto the powder sample through the shafts (including attritor, roll, and pan mills), and in the latter, initially, KE is imparted into the body of the mill and then is transmitted to the balls and samples charged through friction. Examples of indirect mode consists of the planetary, tumbler, and vibratory mills. From the literature, it is evident that the specific energy supplied to the mill charge could be rated planetary > vibrational > attritor > tumbling mill [30].

### 2.3. Based on Wettability

Based on wettability, ball mills are classified into dry and wet mills. In wet ball mills, a surface-active media is introduced to inhibit the formation of aggregates while dry mills are free of solvents and the attrition of particles occurs through powder-to-powder friction. Dry balling is the usual method adopted for the synthesis of carbon nanotube-based composites to control the length of the tube, for stable coatings with strong interface interactions [31–33]. From the earlier investigations, it is evident that wet milling is the effective method for the homogeneous dispersion of ceramic particles [34]. Zhang Z. et al. successfully introduced the structural water into the MnO<sub>2</sub>/Graphite nanocomposites cathode for zinc-ion batteries, which reduces the electrostatic interactions promoting the diffusion of zinc-ions [35].

### 2.4. Plasma Assisted Milling (P-Milling)

Nowadays, in ball milling process, magnetic, ultrasonic, electric energy fields, and temperature are applied. Plasma assisted milling technology, known as p-milling, involves introduction of dielectric barrier discharge plasma in the milling process for improving the milling efficiency, capacity, and process controllability. This involves concurrent action of heating by plasma and the impact resulting in ball-milling for material processing. Plasma is considered to be the fourth state of matter, and is composed of positive ions, neutral particles, electrons, and free radicals. The high energy possessed by these particles and ions can effectively interact with materials. Moreover, p-milling results in the formation of fractures, chemical decomposition, and recrystallization on materials leading to increased surface area formation and different bulk defects compared to conventional ball milling. Hence, they become more attractive in materials processing. Therefore, plasma assisted milling techniques have received significant research interest and are explored for the synthesis of electrode materials, graphene materials, lubricating materials, cermet materials, and hydrogen storage materials [36].

The p-milling route increased the synthesis efficiency of aluminum nitride (AlN) nano powders and reduced the precursor temperatures significantly [37]. The effect of precursors Al<sub>2</sub>O<sub>3</sub> and Al<sub>2</sub>O<sub>3</sub>/C on AlN nano powder synthesis were investigated. Compared with conventional milling (c-milling), p-milling reduced the calcination temperature due to synergistic effects between rapid heating by plasma and impact stress of milling thereby improved the synthesis efficiency.

Sun et al. fabricated nano silicon/graphene nanocomposites as anode materials by embedding nano silicon in graphene using p-milling method [38]. This route converted graphite into graphene nanosheets with the integration of nano silicon in the in situ formed graphene. Twenty hours of p-milling of nano silicon/graphene nanocomposite resulted in a unique structure with homogeneous distribution of nano silicon along with abundant nano-sized free spaces in the composite yielded enhanced conductivity and cycle performance. In another study, lithium storage performance of MgB<sub>2</sub> is investigated [39]. A composite consists of MgB<sub>2</sub>/expanded graphite/TiO<sub>2</sub> is fabricated by p-milling for about 20 h and the resultant composite material exhibited a discharge capacity of 305.5 mA h g<sup>-1</sup>, even after 100 cycles. A facile route for the synthesis of germanium nanoparticles wrapped with few-layers of graphene by plasma assisted ball milling for anode applications is presented [40]. The precursor materials used are commercial grade germanium powder and natural graphite. The electrodes made using germanium/graphene nanocomposite material showed better electrical conductivity, low initial loss, and better cycling capacity compared to conventional milling process.

Although plasma assisted milling is reported to have several advantages, there is also room for discussion and improvement. Owing to the complexity and non-thermal equilibrium nature of plasma, it is difficult to monitor/measure the active particles, such as ions and free radicals, that are present in it and how they affect the materials properties. Secondly, the effect of plasma on the formation of any intermediate products during the course of milling and their effects on mechano-chemical properties of materials is yet to be studied.

### 2.5. Microwave-Assisted Ball Milling

Solid–liquid ball milling is the foundation of microwave-assisted ball milling, which uses a ball milling machine inside a microwave oven (Figure 3). Due to unique microwave effects, microwave heating can accelerate chemical reactions, and high-energy ball milling can successfully stop grain development and purify crystalline particles. The solvent to be used is deionized water, which reduces the reaction time and avoids the use of a significant amount of organic solvent and will have the least negative environmental effects. As a result, it is evident that the adsorbent’s production cost can be reduced.

Without the use of a protective environment, microwave sintering at a milled power of 600 W was successful in synthesizing a Fe-Al<sub>2</sub>O<sub>3</sub> nanocomposite in 15 min [41]. The findings demonstrate that during the microwave-assisted ball milling process, the epoxy ring opens, and epoxy resin molecules were grafted onto the surfaces of nanotitanium hydride (TiH<sub>2</sub>) particles, improving the compatibility between the nanoparticles and epoxy resin [42]. The processing of nano-reinforced aluminum alloy composites involves the incorporation of nano alumina by the use of milling, followed by heat treatment with microwave assistance. The addition of nanoalumina to the grain interface increased the activation energy at the grain interface, causing homogeneous nucleation, which produced an ultrafine-grained microstructure and significantly improved the mechanical properties of the fabricated nanocomposites, such as microhardness and strength [43]. The preparation of vanadium and chromium carbides nanocomposite and their alloys using a novel technique of in-situ microwave heating. The nanocomposite was employed to prevent grain growth in cemented tungsten carbides in its as-prepared state. A well-dispersed nanocomposite with a mean diameter of around 30 nm can be produced at lower temperatures. The alloys’ microstructure and characteristics are significantly impacted by the synthesized nanocomposite [44].

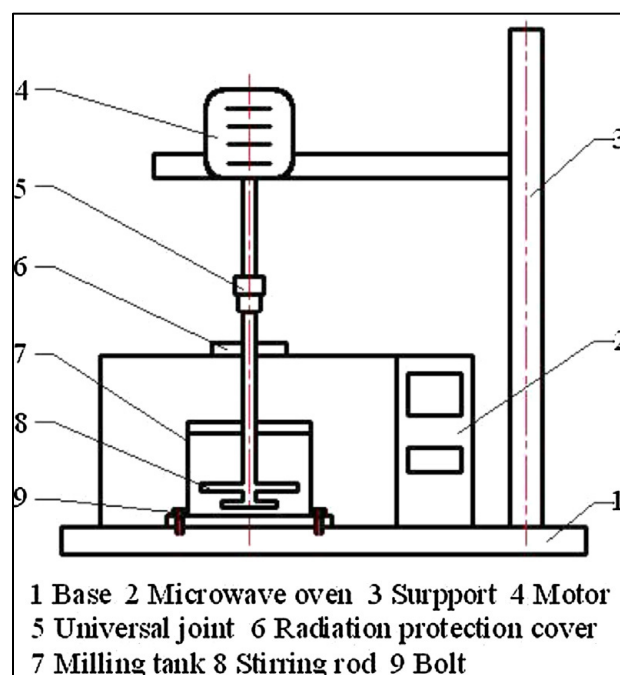


**Figure 3.** Schematic of Microwave-Assisted Ball Milling. “Reprinted/adapted with permission from Ref. [42]. 1999, Elsevier Publications”. More details on “Copyright and Licensing are available via the following link: <http://creativecommons.org/licenses/by/4.0/> (accessed on 29 August 2022).

### 2.6. Electrical Discharge Milling

Long-term conventional milling in an inert atmosphere typically results in the development of porous powder aggregates with small amorphous or irregular particle sizes making up each particle nanocrystalline component after prolonged grinding. The process

of agglomeration used was believed to result from repeated deformation, fracture, and cold welding of elements. During milling, powder particles are repeatedly deformed and fractured, which starts solid–solid, solid–liquid, and solid–gas processes. Reacting a material in a gas environment with an electrical discharge is a different material synthesis and processing method. While milling, the use of low-current, high-voltage electrical impulses can lead to quicker reactions as well as new synthesis and processing pathways. Spark/electrical discharge milling, as opposed to traditional milling, was discovered to cause the formation of amorphous powder with primarily single, sub-micron-sized particles. The structure of individual particles ranged from re-melted particles to sub-micron and irregularly shaped particles, based on the vibrational amplitude choice made during discharge. Large vibrational amplitudes and a broader variety of particles are created with increasing energy input. These included nano-sized particles formed as fume and collected during discharge milling under flowing argon. They also contained sub-micron particles, remelted particles, and welded agglomerates.

Micro-gaps between moving and/or vibrating balls, and between the balls and the milling chamber wall, happen during the process of milling. These micro-gaps can cause an arc discharge or a discharge that is primarily of the glow discharge type. It was discovered that spark discharge milling promotes quick fracture, recrystallization, mineral reduction, and solid–solid reactions, whereas glow discharge milling promotes solid–gas interactions [45]. The findings demonstrate that this approach greatly improves traditional milling in terms of surface roughness [46].

### 2.7. Magnetic Field Induced Ball Milling

Ball milling is a simple and convenient method for the preparation of powders, alloys, and composite materials. This technique results in products having very fine particle size and grain size. Anisotropic magnetic particles with nanosized grain structures can be fabricated by ball-milling under a magnetic field [47]. The structural and magnetic characterization results of sub-micron sized particles obtained by ball-milling in a magnetic field environment unveil strong magnetic anisotropy.  $\text{Sm}_2\text{Co}_{17}$  is considered as a building block for future high performance permanent magnets. Anisotropic  $\text{Sm}_2\text{Co}_{17}$  nano-flakes with high aspect ratio and a thickness of tens of nanometres were synthesized in the presence of heptane and oleic acid by magnetic field induced high energy ball milling [48].

The application of a magnetic field on the morphology, structure, and magnetic properties of ball milled  $\text{TbFe}_2$  alloy was investigated [49]. Researchers found that the rate of particle size reduction in presence of magnetic field was superior compared to simple ball milling. Further, the coercivity of field assisted (magnetic) particles are as high as 6500 Oe whereas it is 3850 Oe only in the absence of magnetic field.

Powder based alloys of  $\text{NdFeB}$  and  $\text{SmCo}$  are produced in a ball mill kept in a uniform magnetic field [50]. The duration of milling was 100 h and samplings were performed every 25 h of milling. The particle size of the powder alloy was  $\sim 100$  nm (after 100 h milling) and their grain size was  $< 20$  nm. The remanence ratio of milled alloy under magnetic field was higher than those prepared in the absence of magnetic field. Furthermore, it was evident from XRD peaks that the material prepared by ball milling in presence of magnetic field had better alignment than those produced by conventional ball milling.

### 2.8. Ultrasonic Milling

Mechanical alloying by ultrasonic milling benefits the combined advantages of ultrasonic, mechanical, and cavitation processes on powder materials that leads to diffusion, mass-transfer, and solid-phase reactions [51]. In this technique, cavitation process plays a vital role in grain size of metal powders or alloys. Compared to conventional milling in planetary ball mills, it is possible to make pseudo alloys from immiscible components, initiate phase transformations and substitution and interstitial reactions in a much shorter time by ultrasonic assisted milling. Schematic illustration of a typical ultrasonic ball mill is shown in Figure 4.

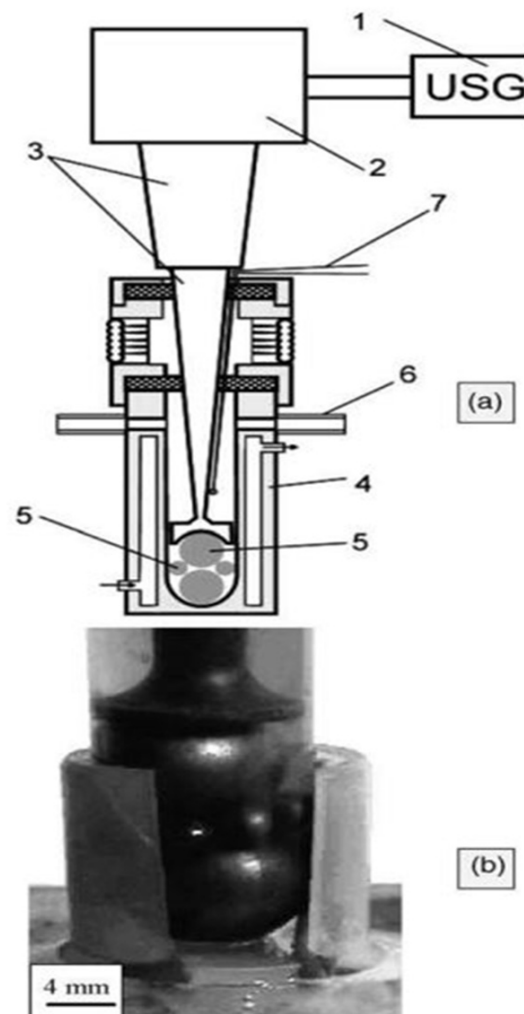


**Figure 4.** Laboratory Ultrasonic grinding mill for powder processing. (a) Scheme: (1) ultrasonic generator; (2) vibrator; (3) step like horn; (4) container; (5) metallic balls; (6) gas inlet; (7) thermocouple. (b) Photo of chamber with transparent walls. “Reprinted/adapted with permission from Ref. [42]. 2004, Elsevier Publications”. More details on “Copyright and Licensing are available via the following link: <http://Creativecommons.org/license/by/4.0/> (accessed on 29 August 2022).

A simple, economic, and eco-friendly synthesis of manganese ferrite nanoparticles ( $\text{MnFe}_2\text{O}_4$ ) with a mean particle size of 20 nm without calcination (low temperature  $\leq 100^\circ\text{C}$ ) by ultrasound wave assisted ball-milling is reported [52]. Iron balls with diameters of 1.0–1.5 mm were used for milling. Ultrasonic ball milling technology was employed for the synthesis of large, ultra-thin, 2D materials: h-BN, graphene,  $\text{MoS}_2$ ,  $\text{WS}_2$ , and BCN. The sizes ranged from 1 to 20  $\mu\text{m}$ , thickness of  $\sim 1\text{--}3$  nm, and a yield of over 20% [53].

Jiang et al. studied the dispersion capability of nano  $\text{La}_2\text{O}_3$  suspensions prepared by four dispersion methods, namely, ball milling, ultrasonic, ultrasonic followed by ball milling, and ball milling followed by ultrasonic [54]. The authors declare that the dispersion capability of nano  $\text{La}_2\text{O}_3$  suspensions were superior in the ultrasonic followed by ball milling method. Through this route, the secondary aggregation of nanoparticles can be minimized, and the aggregates formed if any can be de-agglomerated. They assessed the dispersion stability through particle size analysis (DLS), zeta potential, sedimentation test, and transmission electron microscopy (TEM). Recently, oleic acid modified graphene was dispersed in oil by ultrasonic assisted ball milling and are thickened by a lubricating grease [55]. The graphene modified lubricating grease exhibited improved corrosion resistance and tribological properties. The lubrication mechanism and corrosion resistance mechanism also discussed.

Ultrasonic assisted ball milling for Congo red (azo dye) degradation in wastewater is studied [56]. The researchers used ultrasonic cavitation and mechano chemistry for dye degradation. The effect of zero valence iron significantly increased the hydroxyl radical concentration. By reacting with nano iron, the oxidation of hydroxyl radical accelerated and 99% degradation of dye happened in 2 min. Most of the organic matter was converted into minerals and removal rate of total carbon (TOC) reached 80% within 10 min.

### 2.9. Temperature Assisted Ball Milling In-Situ and/or Ex-Situ

Thermal changes in a ball milling process often influence the diffusivity and defect concentration that may directly impact the phase formation and transformation [57]. Higher temperatures, therefore, result in phases with higher atomic mobility in inter-metallic alloys, whereas, at lower temperatures, the amorphous or nanocrystalline phase formation are inevitable [58]. Macroscopic temperature developed during ball milling has been experimentally measured. Davis et al. [59] and McDermott et al. [60] reported the temperature increase of 40–50 °C in a spex ball mill; however, Kimura et al. [61] and Cabanas-Moreno et al. [62] measured the temperatures range of 172–215 °C, respectively, in an attritor ball mill using SiC and diamond sensors. The macroscopic temperature variations of the ball mill are, in general, low, and sensitive to the ball milling type and design [63,64]. However, the microscopic temperature of the milled powder is quite high due to the high energy impact that causes amorphization, local melting and rapid solidification [65,66]. These microscopic temperatures have been indirectly inferred via modeling mechanism studies, as well as physicochemical characteristics, such as microhardness, crystallite sizes, structural, and microstructural information of the milled ingredients. The mechanical properties of bulk and nanocrystalline copper alloys by ball milling under room temperature and at lower temperature (cryomilling) have been demonstrated by Bahmanpour et al. [67]. According to this study, about 200 MPa decrease in microhardness was found when the sample Cu-10 wt.% Zn alloy is treated and switched from cryo-temperature to room temperature (Figure 5a), and this observation is correlated with the increase in the crystallite size as shown in Figure 5b. Thus, it is clear that the temperature increase causes higher mobility of deformation that has already been created by the cryomilling.

A very recent study of pre-treatment of the cellulose with liquid nitrogen assisted ball milling, thus enhancing conversion of cellulose structure into chemicals and fuels, namely, glucose and formic acid [67]. The effectiveness in hydrolysis reaction of cellulose into glucose and formic acid in two separate experiments demonstrated that the crystallinity and the molecular weight of the cellulose could be reduced with ease using liquid nitrogen temperature assisted ball milling compared to simple ball milling itself [68]. In another study, the nitridation of Fe powder was examined by three different temperatures, liquid nitrogen temperature, room temperature, and at 200 °C using two different gaseous atmospheres, namely, nitrogen and ammonia [68]. Based on the above experiment, it was concluded that the optimal iron nitride formation when Fe powder was subjected under the ammonia gas ambient and with treatment at room temperature and below (liquid nitrogen). Having seen the advantage of liquid nitrogen temperature assisted ball milling, a novel study using ultra cryo-milling method was devised by mechanically milled the poorly water-soluble drug with dry-ice beads in liquid nitrogen environment in ball mill showed improvement in the solubility with less contamination effects [69]. On the hydrogen storage to form a binary/ternary metal hydride ( $MgH_2/Mg_2FeH_6$ ), a cryo-ball milling was demonstrated with higher hydrogen absorption kinetics due to efficient interface-controlled growth processes [70].

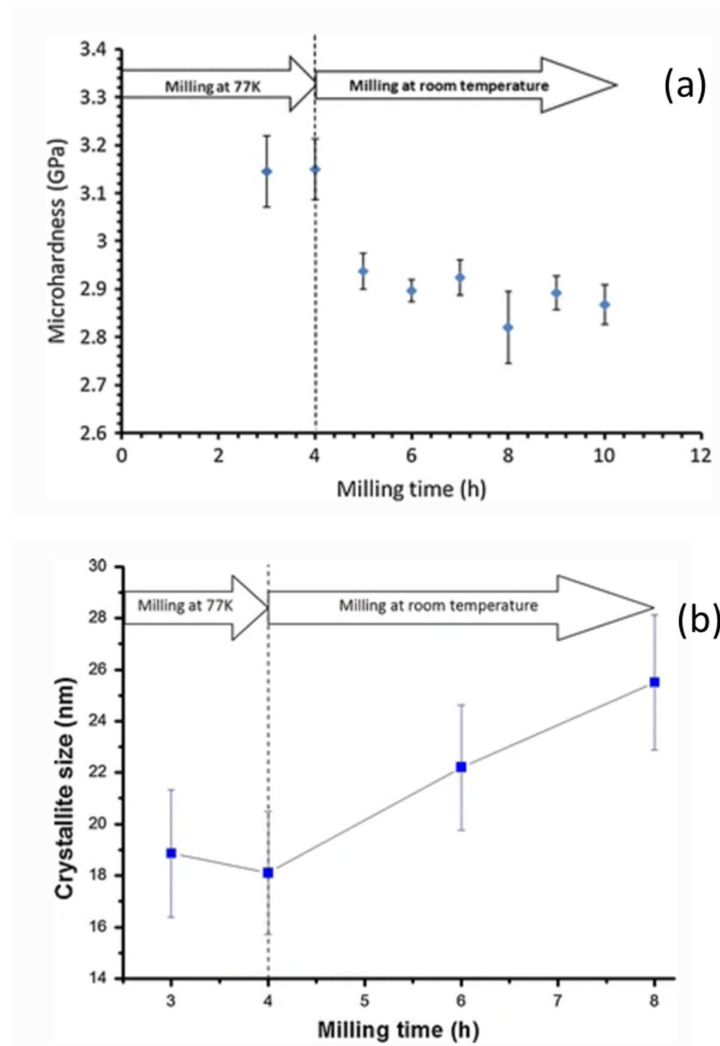


**Figure 5.** (a) Microhardness vs. milling time and (b) crystallite size vs. milling time for Cu-10 wt.% Zn alloy cryomilled for 4 h at 77 K followed by 6 h room temperature milling. “Reprinted/adapted with permission from Ref. [67]. 2011, Springer Nature Publications”. More details on “Copyright and Licensing are available via the following link: <http://creativecommons.org/licenses/by/4.0/> (accessed on 29 August 2022).

### 3. Factors Affecting the Properties of Mechanically Alloyed Nanocomposites

The milling time, rotation speed, milling energy, ball size, and reinforcing material content affect the homogeneity, microstructural, and other properties of mechanically alloyed nanocomposites [71,72].

#### 3.1. Milling Time

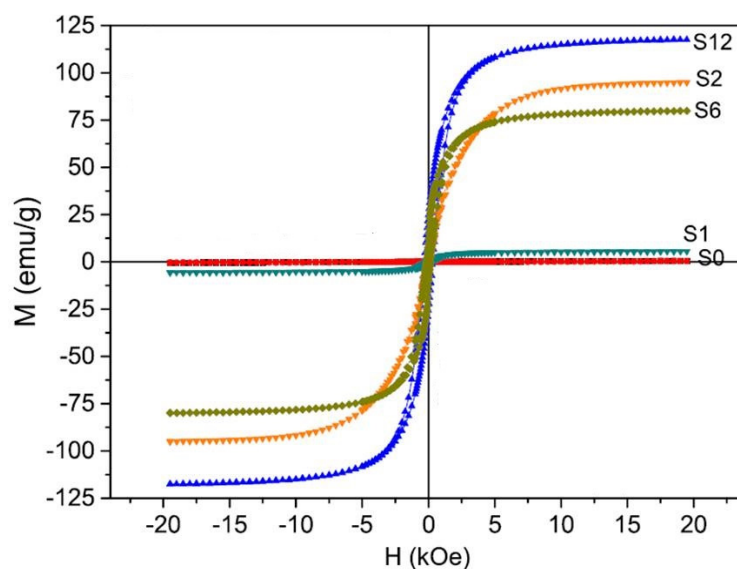
Time duration of milling is a vital parameter in the ball milling process in the phase formation, microstructural distribution, and homogenous distribution of components or ingredients. It also influences the physicochemical-mechanical properties of the composites. The size of the nanomaterial (reinforcing material) reduces with an increase in milling time. The morphological and particle size transformation of nanocomposite material as a function of time of milling is depicted in Table 1. Plastic deformation occurred for  $Mg_{20}SiC$  with a prolonged grinding process, resulting in crystalline defects and dislocation defects [73]. The average size of the crystallites for the Mg material decreased and the powder became finer and equiaxed with the increased milling time. Furthermore, no phase change occurred during milling [71].

**Table 1.** Morphological and particle size dependence of composite as a function of time duration of milling.

Material	Time	Particle Size	Morphology
Mg <sub>20</sub> SiC [71,73]	0	45.56 ( $\pm$ 9.20) $\mu$ m	Spherical
	1 h	42.18 ( $\pm$ 8.78) $\mu$ m	Flattened
	5 h	36.81 ( $\pm$ 8.51) $\mu$ m	Flattened
	10 h	39.98 ( $\pm$ 9.15) $\mu$ m	agglomerated and laminar
	15 h	21.93 ( $\pm$ 6.18) $\mu$ m	Laminar
	20 h	13.84 ( $\pm$ 5.3) $\mu$ m	equiaxed and regular
Graphene [74]	90 min	4 layers	Platelet
	95 min	2 layers	Platelet
	100 min	1 layer (monolayer)	Particulate

With the progression of milling time, graphene transforms from platelet to particulate shape. The reinforced material becomes protected since the particle is embedded on the interface of the matrix and, hence, there is no further deformation introduced onto the nanomaterial. However, this significantly aided the uniform distribution of nanomaterials in the matrix phase. As the milling time increases, there is an enhancement in the mechanical strength and flexural strength. With shorter milling time, there is a chance of agglomeration as the time increases the chance of agglomeration weakens, and, therefore, improved mechanical property could be observed [74].

Studies suggested that the magnetic properties also increase with the progression of milling time. As shown in Figure 6, Co/Al<sub>2</sub>O<sub>3</sub> nanocomposite initially showed feeble ferromagnetism, while after increasing the milling time to 12 h, it revealed a strong saturation magnetization of 118 emu/g [75].

**Figure 6.** Magnetic hysteresis loop of Co/Al<sub>2</sub>O<sub>3</sub> nanocomposite after milling time (0 h (S0), 1 h (S1), 2 h (S2), 6 h (S6), and 12 h (S12)) [75]. (RightsLink Printable License obtained to use this Figure from Elsevier Publications, Ceramics International).

### 3.2. Milling Speed Cum Energy

Milling speed significantly influences the particle size and grain boundary size. With the increase in milling speed, there was a consequent reduction in the size of the particles [76]. It was found that CNT nanoparticles share a feeble interfacial bonding with the

Cu surface at a low rotation speed [77]. The crystalline size of the particles reduced subsequently with the increase in milling speed (Figure 7). The surface defects and roughness were minimal at low milling speed, while high milling speed attributed to higher strain hardening and thermal softening [78].

Relatively, high milling energy is required for well distribution and dispersion of nanofiller into the matrix. The high energy milling attributes to reduced crystalline size in dry milling, while wet milling does not show much effect due to the presence of a solvent [79].

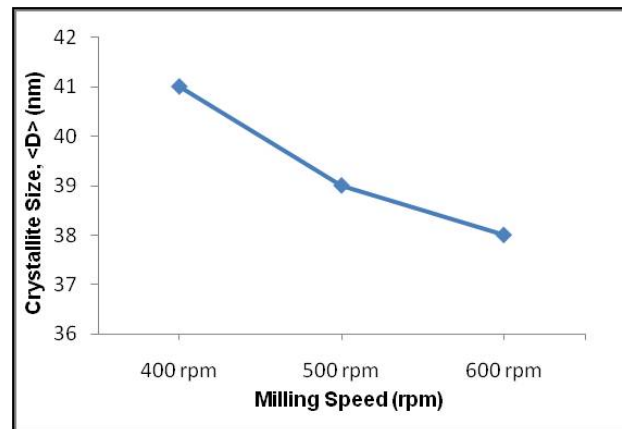


**Figure 7.** The effect milling speed on crystal size [80] (Permission obtained to use the figure from UTM eJournal Editorial Team via email).

### 3.3. Ball Size

The size of the balls used for milling have a greater impact on the crystal size, yield of production, and energy consumption. The efficiency of the milling increases with smaller diameter balls (sized 10 mm or lesser) (Figure 8); the ball to grinding media contact points increases, leading to a higher number of collisions and exerts a higher shearing force. This increases with an increase in time [81]. In contrast to this, when the size increases, the weight of the ball also increases, which infuses greater kinetic energy. The kinetic energy has a direct impact on the ball size. As the size of the balls increases, the amount of free space also increases exponentially; this could be resolved with a mixed ball size combination [82].

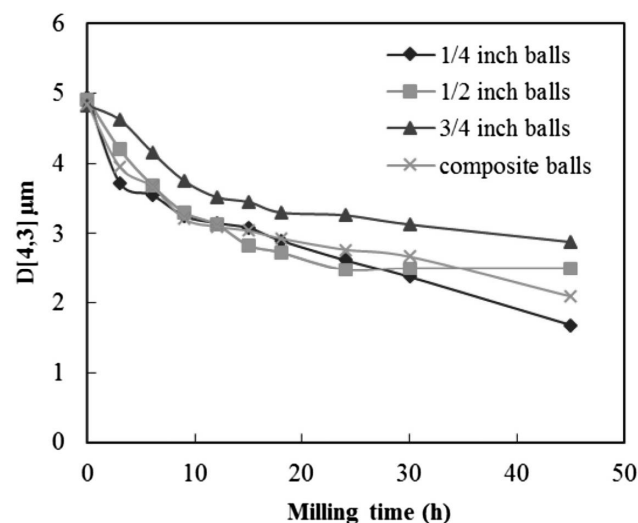


**Figure 8.** Effect of size of the balls on particle diameters as a function of milling time [82]. (RightsLink Printable License obtained to use this Figure from Springer Nature Publications, Transactions of the Indian Institute of Metals).

### 3.4. Concentration of Nanomaterials

The higher concentration of reinforcing material leads to higher deformation and micro hardening of the matrix phase. This accelerates the fracturing and welding processes and promotes the process of milling to be completed in a briefer duration since the grain growth of metal is inhibited by the nanoparticles [3]. If the content exceeds a certain amount, that will introduce failure into the composite system [83]. The microhardness of Fe-MWCNT increases up to 2 wt.% of MWCNT, beyond which there was a decline in the hardness. The conductivity of the composite increases to 3 wt.% and then decreases. These effects are due to the agglomeration that causes enlargement of MWCNT, which induces a longer pathway for the electrons to pass through, entraps the micropores, and also lowers the aspect ratio of MWCNT causing reduced bonding between the metal host and the MWCNT [13].

### 3.5. Ball to Powder Ratio

The ball-to-powder ratio is an important and fundamental parameter of milling operations. However, other factors cannot be neglected in the high energy ball milling processes of materials. P. Kuziora et al. checked the effect of constant ball-to-powder (BPR) on a few powder samples of  $MgH_2$  for hydrogen desorption properties [84]. The authors depicted interesting results for the specific parameters that the same BPR does not create the similar microstructure on the contrary filling of vial is the most affected factor for change in various physical properties. Z.M. Wu et al. applied BPR model for the refinement of microstructure of Tungsten [85]. In this work, researchers fabricated samples by changing ball-to-powder ratio and compared those by means of various structural tools. The interesting part of the research is that the ball-to-powder ratio of 15:1 impacted more on particle size than lower BPR. Hence, more BPR reduces the particle size up to nano regime.

### 3.6. Energy Dose

Energy Dose is a vital parameter that is expressed as an energy transfer per mass unit of milled constituent powder [86]. All of the above-mentioned factors in Sections 2.1–2.5 that are actually correlated to the energy dose based on the milling devices. For example, in terms of ball-to-powder ratio, that may alter the energy intensity because the intensity of milling is directly proportional to the kinetic energy ( $E_k$ ), number of balls ( $N$ ), and the impact or hits per unit time ( $F$ ). Similarly, the energy dose is the product of energy intensity with the time of milling to an amount of material powder ( $P$ ). Overall, the energy dose is quantified by understanding the various milling parameters, such as impact velocity, impact frequency of the balls, charge ratio, and the vial filling ratio [86]. It has been very recently reported that the kinetic energy dose can be used as a unified metric for comparing ball mills in the case of mechanocatalytic depolymerization of lignocellulose [87].

## 4. Synthesis and Characterizations of Ball Milled Variants

### 4.1. Synthesis of Metallic Nanocomposites

The ball–powder–ball collision is an un-denying factor that governs the mechanochemical alloying process. Initially, the chemical ingredients are smashed between the balls during continuous collision. Secondly, the sequence of materials' deformation and/or fractures occur that decides the structure of the final product. It is noteworthy to mention that the overall mechanochemical processes rely heavily on the physicochemical characteristics of the constituent chemical ingredients, their phase and/or interface equilibria, and stress–strain properties in the prolonged milling process. Therefore, the final product from the ball milling procedure depends on the permutation and combinations of the different properties such as ductile–ductile, ductile–brittle, and brittle–brittle. As mentioned above, the sequential or parallel processes that involve for the mechanochemical milling are: (i) the local temperature rise induced coalescence and/or fragmentation effects, (ii) deformation at the microscale that causes defects and dislocations in free volumes, (iii) deformation at

the surface due to catalytic effects, and (iv) stress increase on the powders while milling due to hydrostatic variations.

#### 4.2. Synthesis of Non-Magnetic Metallic Nanocomposites

Jargalsaikhan et al. [88] fabricated Al/CNT nanocomposite using a planetary ball milling followed by sintering. The dispersion of CNT in Al and the mechanical behavior and hardness of the composite nanostructures were evaluated. Milling was carried out at 100 and 150 rpm rotating speed for 5 and 15 min with a 10:1 ball to powder ratio using zirconia balls. The milled composite was then subjected to calcination at 500 °C for 5 h and was cooled at room temperature. CNT was well-dispersed homogenously into the Al surface and resulted in enhanced mechanical strength and hardness. As inevitably demonstrated in Figure 9, the mechanical hardness increased at least 40–60 HV values for the Al/CNT nanocomposite ball milled when compared to un-milled or milled Al samples.

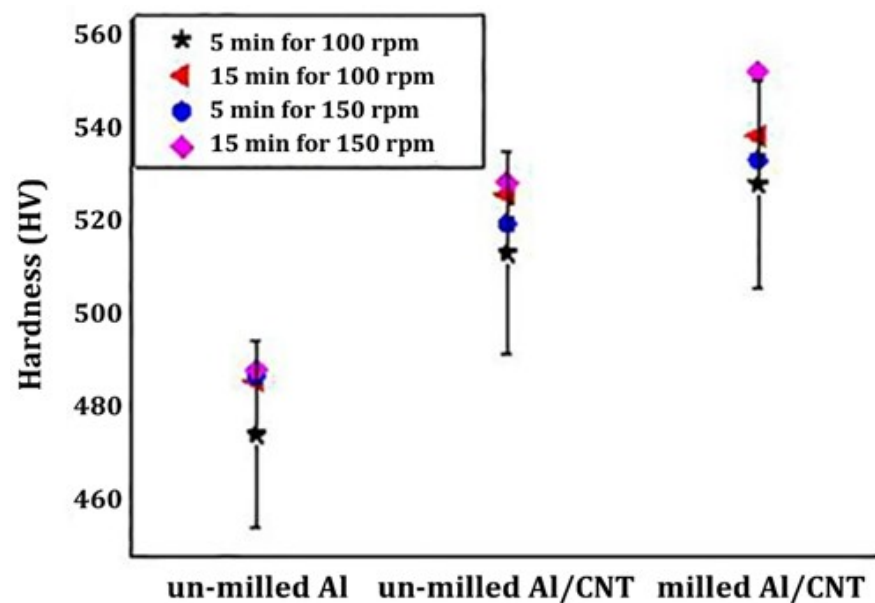


**Figure 9.** Hardness of Al/CNT nanocomposite [88]. (Permissions to use this Figure is granted since the source article is an open access distributed under the terms and conditions of the Creative Commons Attribution (CC By) license (<http://creativecommons.org/licenses/by/4.0/> (accessed on 26 July 2022))).

Fathy and co-workers [89,90] aimed to investigate the effect on the properties of ball milling ZrO<sub>2</sub> nanomaterial in the Cu matrix. Cu and ZrO<sub>2</sub> powders were ball milled at a rotating speed of 250 rpm and were cold-welded and calcined at 950 °C for 2 h. The microhardness increased up to 288%, the compressive strength increased with the decrease in crystalline size, and the electrical conductivity decreased with higher ZrO<sub>2</sub> contents.

Zawrah et al. [91] embedded Cu particles onto Al<sub>2</sub>O<sub>3</sub> nanocomposite using a planetary ball mill. Process controlling agent was added to avoid agglomeration during the milling process. Uniform dispersion of Cu over Al<sub>2</sub>O<sub>3</sub> was obtained with higher fracture strength. These studies show that the nanocomposites between materials that have very different chemical and physical identity can be successfully synthesized using ball milling technique.

#### 4.3. Synthesis of Magnetic Nanocomposites

High energy ball milling not enhances the surface properties like active surface area, pore size, pore volume, and bulk density, as well as the magnetic properties of nanocomposites. The magnetic property of nanocomposite depends upon the coupling of the soft and hard phases of the material. It not only depends upon these intrinsic properties, but also on the microstructure and grain size. This helps in achieving high remanence and coercivity. Multiferroic systems can also be obtained by mechanochemical milling [92]. High energy

ball milling and spark plasma sintering methods were utilized by Zhuge et al. [93] to prepare  $\text{SmCo}_7/\alpha\text{-Fe}$  magnetic nanocomposite.  $\alpha\text{-Fe}$  nanoflakes were mixed with  $\text{Sm}_2\text{Co}_7$  ribbons and were subjected to high energy milling, and then hot-pressed using spark plasma sintering. To investigate the effect of inter-granular exchange in magnetic properties, the hard ( $\text{SmCo}_7$ ) and soft phases ( $\text{SmCo}_5$ ) were compared and found that the hard phase showed a better exchange coupling effect as it increases the exchange length. It was found that magnetic field heating after high energy balling, improves the remanence and coercivity of  $\text{SmCo}/\alpha\text{-Fe}$  nanocomposite magnets. The remanence and coercivity were improved by 17% and 23%, respectively [94].  $\text{SiO}_2$ ,  $\text{Fe}_2\text{O}_3$ ,  $\text{NiO}$ , and  $\text{ZnO}$  have been milled together to synthesize  $\text{NiZn}$  ferrite/ $\text{SiO}_2$  nanocomposites at 10:1 ball to powder ratio and at a speed of 200 rpm for 1 to 250 h, and heat treatments have been performed to obtain nanocomposites having highest saturation magnetization and coercivity [95]. The  $\text{NiZn}$  Ferrite/ $\text{SiO}_2$  are at least two orders of magnitudes superior to their pristine counterparts.

Chen et al. [96] reported the preparation of  $\text{SmCo}_5/\alpha\text{-Fe}$  magnetic nanocomposite with different La/Ce substitution concentration by high energy ball milling followed by calcining at 450 °C to 650 °C for 30 min. The powder to ball weight ratio was 1:25. The X-ray diffraction (XRD) pattern was used to estimate the phase structure of La and Ce doped nanocomposite magnet at different dopant content and annealing temperatures (Figure 10). There was no change in the hard phase with the increased Ce content and elevated temperature in the magnetic nanocomposites, while a transition change was observed with the higher La content and annealing temperature. The magnetic property was studied using a vibrating sample magnetometer. In fact, the increase in La or Ce dopants decrease the magnetization performances of the host material,  $\text{SmCo}_5/\alpha\text{-Fe}$ . The hysteresis loop (Figure 11) exhibited strong ferromagnetism for both Ce and La-doped nanocomposite. Additionally, the magnetic performance was found to be higher for the La-doped,  $\text{SmCo}_5/\alpha\text{-Fe}$  nanocomposite compared to that of the Ce-doped magnetic nanocomposite.

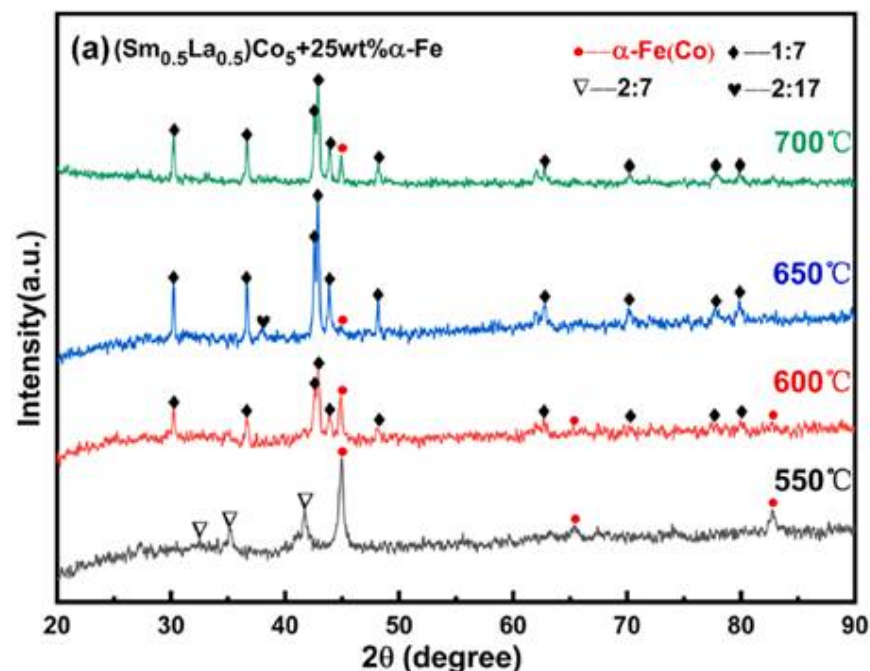
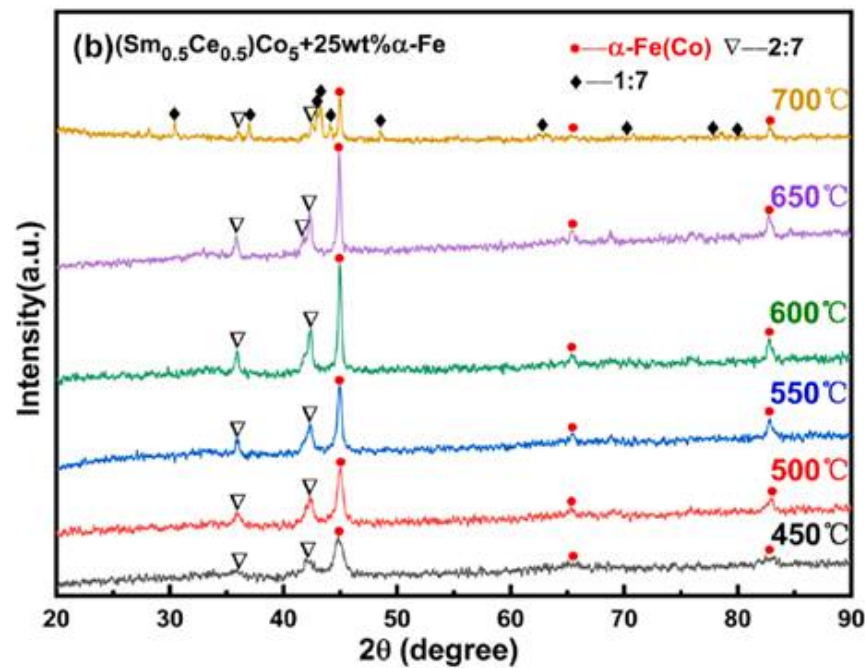
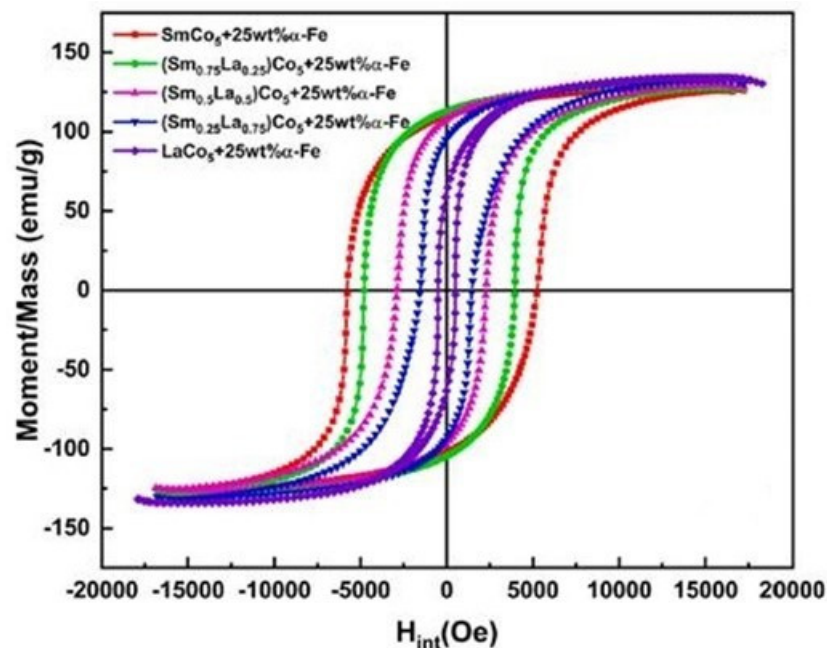


Figure 10. Cont.



**Figure 10.** XRD patterns of (a) La-doped  $\text{SmCo}_5/\alpha\text{-Fe}$  (b) Ce-doped  $\text{SmCo}_5/\alpha\text{-Fe}$  at different annealing temperatures [96]. (License obtained to use this Figure from Elsevier Publications, Journal of Magnetism and Magnetic Materials).



**Figure 11.** Hysteresis loop of  $\text{SmCo}_5/\alpha\text{-Fe}$  magnetic nanocomposites [96]. (License obtained to use this Figure from Elsevier Publications, Journal of Magnetism and Magnetic Materials).

#### 4.4. Synthesis of Polymer Nanocomposites

Ball milling in polymers helps in the chemical transformation of many block polymers under mechanical agitation even without the presence of solvents. The most common method of mechanical alloying is via the wet milling process, where the polymer is dispersed/dissolved in the solvent [97]. González-Benito et al. [98] reported the production of nanocomposites using poly(vinylidene fluoride) (PVDF) by high energy ball milling and subsequent hot pressing. The pulverization was carried out under cryogenic conditions for an hour with intermittent breaks. This allowed homogenous dispersion of barium titanate

and MWCNTs into the polymer matrix, which enhanced the permittivity and decreased the dielectric loss of PVDF without compromising the piezoelectric characteristics. Tanna et al. synthesized  $\text{Ca}^{2+}$ - $\text{Zr}^{4+}$  doped  $\text{BaTiO}_3$  and checked the effects of high energy mechanical milling on the hysteresis and dielectric behavior of these ferroelectric materials [99]. The authors observed interesting results on PE hysteresis loops and dielectric parameters via high energy mechanical milling for various duration with respect to particle sizes of the treated specimens.

Wu et al. [100] developed a one-pot in situ method for the synthesis of polymer/graphene composite with the support of wet ball milling and hot pressing. The solution of ultrasonicated maleic anhydride grafted poly (ethylene-co-vinyl acetate) and graphene was subjected to ball milling for 30 h at a speed of 300 rpm. The decomposition temperature of the polymer nanocomposite was found to be much higher.

Physical and chemical modifications enhance the physicochemical properties of starch by controlling its microstructure [101]. Dai et al. [102] developed starch nanocrystal by mechanical alloying pretreatment to prevent it from damage during the hydrolysis process. The pre-treated starch nanocrystal was then hydrolyzed using sulfuric acid. The hydrolysis took less time and produced a higher yield as a function of time duration of milling, as shown in Figure 12.

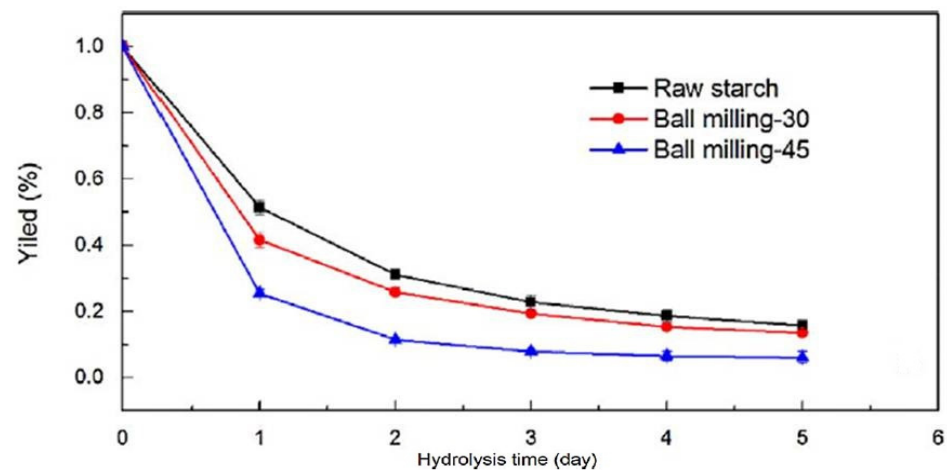


**Figure 12.** The yield % of hydrolyzed starches as a function of ball milling times (0, 30 and 45 min) during the 1–5 days of hydrolysis's period [102]. (RightsLink License obtained to use this Figure from CCC, Copyright Clearance Center, Carbohydrate Polymers).

In a work by Yu et al. [103], the hexagonal boron nitride and the polydopamine solution were mixed ball milled at 400 rpm for 24 h; further cellulose nanocrystal was added obtaining higher thermal conductivity as shown in Figure 13. Yang et al. [104] examined the interfacial interaction and mechanical properties of PBT/nano- $\text{Sb}_2\text{O}_3$  composites. Poly(butylene terephthalate) (PBT) and the additives were first dispersed by a high-speed rotating (HSR) mixer before being introduced into the planetary ball mill and milled at 300 rpm for 6 h. Homogenous dispersion of nanofiller in the polymer was obtained by high energy ball milling (HEBM) as compared to the high-speed rotating mixer as evident from Figure 14. Moreover, it exhibits good interfacial interactions which improved the mechanical strength of the nanocomposite. In the successive studies by Lie et al. [105], preparation of PBT/nano- $\text{Sb}_2\text{O}_3$  composites by high-energy ball milling (at 400 rpm for 6 h) and subsequent melt blending process could observe an improvement in the flammability and mechanical properties.

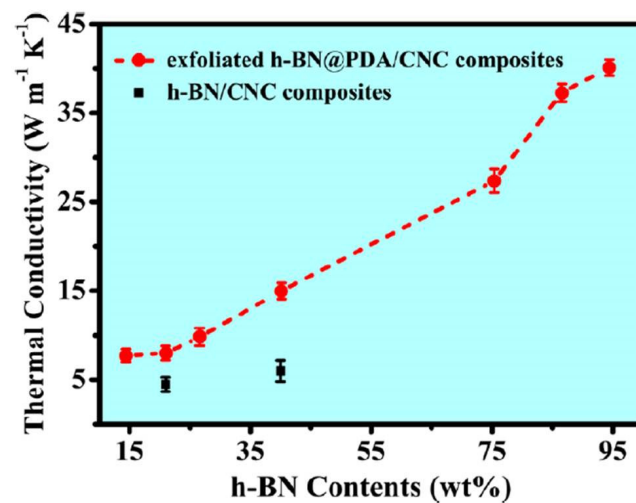


**Figure 13.** Thermal conductivity of exfoliated h-BN@PDA/CNC composite and h-BN/CNC composites [103]. (RightsLink License obtained to use this Figure from CCC, Copyright Clearance Center, ACS Publishers, ACS Applied Nanomaterials).

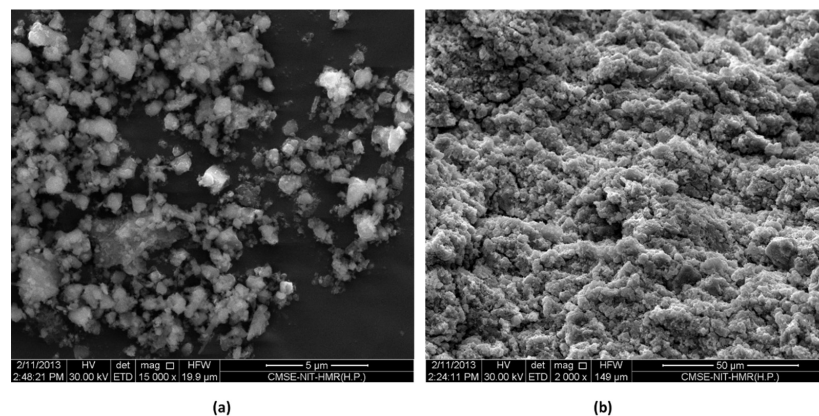


**Figure 14.** SEM images (a) HSR and (b) HEBM.

#### 4.5. Ceramic Nanocomposites

Hannora and Ataya [22] prepared hydroxyapatite/titania nanocomposites by high energy ball milling using hardened steel balls for 1 h. The sample was then cold-pressed and consolidated at different sintering temperatures and analyzed the decomposition and phase changes. The resultant specimen showed deformities with higher compression stress.

Sharma and Dalvi [106] proposed a novel method to prepare  $\text{LiTi}_2(\text{PO}_4)_3$ -glass-ceramic nanocomposites utilizing the mechanical alloying technique. At first, the powder mix was ball milled for 6–18 h in acetone medium at 400 rpm and alloyed for 1 h at 100 rpm before being hydraulically pressed. To acquire a higher melting point, it was again heated and quenched. Thus, prepared composite exhibited high electronic transport property.”

## 5. Applications

### Energy Storage

The conventional energy sources are depleting rapidly and alongside creating several environmental issues such as global warming, air pollution, rising sea levels, thinning of ozone layer, etc., renewable energy sources, such as solar energy, hydropower, geothermal energy, ocean energy, etc., can help in meeting the energy demands of human society. However, high volatility, irregularity, security, and storage issues make it difficult for their global commercialization. To resolve these issues, researchers propose novel functional materials for efficient energy storage, which is reliable, cost effective, environmentally friendly, and is available easily and for long-term use. Until now, many materials and

compositions, such as nanocomposites, ceramics, and carbon-based composites, have been tested in this regard. Lithium-ion batteries and supercapacitors have shown promise in energy storage devices in modern technologies due to their higher energy density, faster charging, and lower discharging rate, longer cycle life, and wide operating temperature ranges. In these energy storage devices, the active electrode materials play a crucial role as they directly participate in the electrochemical charging–discharging reactions.

There are numerous synthesis techniques, such as hydrothermal route [107,108], microwave synthesis method [109,110], chemical vapor deposition technique [111,112], etc., that have been used for synthesizing materials which have demonstrated enhanced energy storage capacity. Ball milling is one of the synthesis techniques that belongs to the class of mechanochemical processes for synthesizing micro and nano structured materials. Large scale production is one of the major advantages of this technique. Ball milled materials that include metal nanocomposites, ceramic composites, carbon-based materials, etc., are reviewed that have demonstrated satisfactory performance in energy storage mainly as metal-ion batteries like Li, Na, K, and supercapacitors and partly as hydrogen storage, thermal power storage materials, etc.

Fuel cells as energy conversion devices and batteries or supercapacitors as energy storage devices are currently the thrust areas in the domain of energy research. The options of hydrogen production and hydrogen storage areas are also emerging as allied fields. Fuel cells and batteries have certain challenges in terms of reaction kinetics or energy and power density targets to be met, while in hydrogen storage, the uptake capacity as well as rate of adsorption/desorption matters. In case of the proton exchange membrane (PEM) fuel cells, the oxygen evolution and oxygen reduction reaction (ORR) should be effective reactions for a competitive cell performance. These are governed by the interactions between the nanomaterials of the electrodes and electrolytes (or gases) and, thus, the interfacial interactions become very important. In view of this, energy conversion and energy storage processes heavily depend upon the type of material, size of material, its phase, interconnections, conduction channels, bonding strengths, bonding environment, etc., as they either promote or disrupt the flow of charges in one way or the other. The techniques employed for synthesis of nanomaterials thus influence the performance of the device considerably. One of the distinctive properties of a ball-milling technique is the slow transformation of starting material into the final nanomaterial following a top-down approach. In this method, the phase changes occur gradually and at different physical sites of the sample. This inherently creates a host of defect sites in the nanomaterials. Defect sites can act as sites with increased electron charge density or lower charge density and in the process influence the charge transfer process. Some reports where ball milling has been employed for energy storage/conversion are now discussed briefly. A significant increase in the catalytic activity towards oxygen reduction has been observed in the mechanical alloyed GO/ $\alpha$ -MnO<sub>2</sub> nanocomposites due to the chemically stable and mechanically flexible nature of GO nanosheet and porous morphology of  $\alpha$ -MnO<sub>2</sub> nanowire [113]. A cathodic catalyst has significant influence on the power density, cyclic ability, and energy efficiency of batteries. An air breathable composite of nanosheet as matrix and nanowire as transport structure is seen as a promising material for ultrafast Li<sup>+</sup> and electronic charge transportation. The morphology of the cathodic catalyst plays a major role in the enhancement of capacity and reversibility of the Li-O<sub>2</sub> battery. An excellent electrochemical performance was observed in anodic ball milled SnSe/carbon nanocomposite in sodium-ion and lithium-ion batteries [114]. SnS<sub>2</sub>–carbon nanocomposite anode material facilitating a large number of Li<sup>+</sup> ion storage sites, high current density, and faster ion diffusion capability was developed by the facial ball milling process [115]. Table 2 summarizes some recent studies that have employed ball milling technique for processing materials and their subsequent application in the area of energy storage.

**Table 2.** Materials that were processed via ball milling demonstrated better performance as energy storage materials.

Type of Ball Milling	Specification	Battery/Supercapacitor	Highlights	Ref.
Planetary ball mill	Nano sized Mg/nanostructured MgH <sub>2</sub> was obtained by 0–3 h of ball milling the magnesium and benzene in zirconia coated mill pot	Hydrogen storage	<ul style="list-style-type: none"> <li>➤ MgH<sub>2</sub> and benzene ball milled together increases the capacity of hydrogen storage and reversibility</li> <li>➤ Al doped (at 1%) or Ni doped (at 2.9%) with MgH<sub>2</sub> sample exhibits ~60% of hydrogen storage capacity</li> </ul>	[116]
Discharge-plasma assisted milling (Vibration type ball mill)	By taking nano sized Si powder and graphite in mass ratio of 30:70 and ball to powder ratio of 50:1 in P-milling for a time duration of 5,10 and 20 h in presence of pure argon atmosphere to made composite of nano Si and graphene	Lithium-ion battery	<ul style="list-style-type: none"> <li>➤ The composite of nano Si and graphene nanosheets by P-milling with 20 h of duration exhibits 976 mA h/g at 50 mA/g of stable reversible capacity</li> <li>➤ Anode conductivity performance and stability of lithium-ion batteries are improved by nanosheets of graphene with available nanoscale free vacancies on which Si nano particles are homogeneously embedded.</li> </ul>	[38]
Planetary ball mill	180 balls of same size and same materials used in milling of binary fluoride (BaF <sub>2</sub> and SnF <sub>2</sub> ). 17:1 ratio of ball: powder taken with 10 h of milling time	Electrochemical storage	<ul style="list-style-type: none"> <li>➤ Approximately 0.7 mS/cm of change in DC conductivity shown by ternary fluoride (BaSnF<sub>4</sub>) layered structure at ambient temp.</li> <li>➤ Density of mobile charge carriers is a function of temperature shown by different values of low activation energies (~0.27 eV above the room temperature (RT) and ~0.34 eV below RT)</li> </ul>	[9]
Ball milling	Graphite powder and nickel powder were milled using Zirconia balls for 1 h with 1200 rpm.	Supercapacitor	<p>The electrode made by NiO/RGO nanocomposites showed</p> <ul style="list-style-type: none"> <li>➤ 590 F/g of prominent specific capacitance measured at 1 A g<sup>-1</sup></li> <li>➤ Rate of higher capability (88% high retention rate of 15 A g<sup>-1</sup>)</li> <li>➤ Outstanding cycling stability (the retention rate is 100% after 1000 number of charge/discharge cycles)</li> </ul>	[117]
High energy ball milling	Si powder of micro sized dimensions and stainless-steel balls are used in the ball milling with ball: powder ratio of 20:1 at room temperature with different time durations having 1200 rpm rotation speed	Lithium-ion batteries	<ul style="list-style-type: none"> <li>➤ Porous nature of Si electrode with ~20 nm pore size coated with uniform layer of carbon (approx. 4.5 nm) reveals</li> <li>➤ Higher reversibility of 1016.1 at 1000 mA h g<sup>-1</sup> and 834.1 mA h g<sup>-1</sup> at 2000 mA h g<sup>-1</sup> (High cycling stability, &gt;99.5% for 200 cycles)</li> </ul>	[8]

Table 2. Cont.

Type of Ball Milling	Specification	Battery/Supercapacitor	Highlights	Ref.
Ball milling	Si, polycrystalline particles, and waste Si wafers were used in ball milling with 5 h of duration and 1200 rpm speed for grinding the materials	Lithium-ion batteries	<ul style="list-style-type: none"> <li>➤ The outstanding cycling performance (1000 mA h g<sup>-1</sup> after 1000 cycles) was shown by particles prepared by different Si sources</li> <li>➤ The energy density of “lightweight and free-standing electrodes” comprising with Si and carbon nanofibers coated with hierarchical carbon was enhanced by 745 percentages in comparison with conventionally used electrodes</li> <li>➤ The pairing of cathode materials like LiCoO<sub>2</sub> and LiNi<sub>0.5</sub>Mn<sub>1.5</sub>O<sub>4</sub> with the Si based anode exhibits energy density around 547 W h kg<sup>-1</sup></li> </ul>	[118]
Ball milling	The bulk material of MoS <sub>2</sub> and GO were milled for 5 h in 1:1 ratio	Lithium-ion battery and supercapacitor	<p>The organized assembly of MoS<sub>2</sub>/rGO composite electrode exhibits</p> <ul style="list-style-type: none"> <li>➤ 306 Fg<sup>-1</sup> of higher specific capacitance measured at 0.5 A g<sup>-1</sup> of current density</li> <li>➤ Approximately no decay in discharge capacity exhibits for lithium-ion batteries after 100 cycles with 0.2 A g<sup>-1</sup> and for supercapacitor after 5000 cycles with 4 A g<sup>-1</sup></li> </ul>	[119]
Planetary ball mill	The calcium carbide, pyrazine, ethanol, and balls of stainless steel are taken in 1:1:1:1 quantity ratio. Ball milling was performed with 600 rpm for 24 h in argon atmosphere.	Supercapacitor	The rapid electron mobility, electrochemically active larger surface area and defects of nitrogen heteroatomic exhibits higher electrochemical performance with 235 Fg <sup>-1</sup> at 1 A g <sup>-1</sup> of capacitance and retention rate of 87% after 3000 cycles	[7]
Solvothermal-ball-milling	1 h of short time ball-milling was carried out by coating Ketjenblack material on the surface of Na <sub>3</sub> V <sub>2</sub> (PO <sub>4</sub> ) <sub>2</sub> F <sub>3</sub>	Alkaline-ion batteries	<ul style="list-style-type: none"> <li>➤ Na<sub>3</sub>V<sub>2</sub>(PO<sub>4</sub>)<sub>2</sub>F<sub>3</sub> coated Ketjenblack showed 138 mA h g<sup>-1</sup> of specific capacity of at charging/ discharging rates of 1/2 C and 122 mA h g<sup>-1</sup> of capability at 40C, respectively.</li> </ul>	[120]
Planetary ball mill	Specific compositions of Na <sub>2</sub> CO <sub>3</sub> , K <sub>2</sub> CO <sub>3</sub> , Bi <sub>2</sub> O <sub>3</sub> , Ta <sub>2</sub> O <sub>5</sub> , ZnO, and Nb <sub>2</sub> O <sub>5</sub> pure powders were used for synthesis of KNN-BZTN in stoichiometric proportion of 0.925(K <sub>0.5</sub> Na <sub>0.5</sub> )NbO <sub>3</sub> -0.075Bi(Zn <sub>2/3</sub> (Ta <sub>0.5</sub> Nb <sub>0.5</sub> ) <sub>1/3</sub> )O <sub>3</sub> )	Dielectric ceramic capacitors	<ul style="list-style-type: none"> <li>➤ The KNN-BZTN ceramic with ~250 nm of average grain size and large number of amorphous grain boundaries exhibits recoverable high energy density of 4.05 J cm<sup>-3</sup> with 87.4% of energy efficiency.</li> </ul>	[121]

Table 2. Cont.

Type of Ball Milling	Specification	Battery/Supercapacitor	Highlights	Ref.
High Energy Ball Milling (HEBM) (Mixer mill)	HEBM (with 15 Hz frequency 30 min of milling time) executed to make composite of Fe <sub>2</sub> O <sub>3</sub> , MWCNT and PVB in the mass ratios of 80,20 and 3 respectively. (MWCNT-Multiwalled carbon nanotubes and PVB-poly vinyl butyral) along with the gallocyanin	Supercapacitor	<ul style="list-style-type: none"> <li>➤ Three different composites were made for measurement of capacitance of electrodes</li> <li>➤ Composite electrodes were tested for electrochemical performance in 0.5 M of sodium sulfate electrolyte</li> <li>➤ Composite containing HEBM <math>\gamma</math>-Fe<sub>2</sub>O<sub>3</sub>, MWCNT and co-dispersed gallocyanine exhibited 1.53 F cm<sup>-2</sup> maximal capacitance compared to other composites (0.59 F cm<sup>-2</sup> and 0.88 F cm<sup>-2</sup>) for 2 mV S<sup>-1</sup> of scan rate</li> </ul>	[122]
Planetary ball milling (Wet Ball Milling)	Powder samples of few layered graphene (FLG), NbSe <sub>2</sub> (FLN), composite of FLN@ graphene (FLNG) and LiFePO <sub>4</sub> (LFP)@ graphite were prepared with different ratios of powders and different milling conditions.	Lithium-ion and Fuel cell batteries	<ul style="list-style-type: none"> <li>➤ The wet ball milling method was used to prepare the composite of wet ball milled few layered 2D NbSe<sub>2</sub> heterostructures with graphene (WBMNG)</li> <li>➤ Particles of layered NbSe<sub>2</sub> are inserted on the few layered graphene matrix</li> <li>➤ The WBMNG composite exhibited nearly 1142 and 1000 mA h g<sup>-1</sup> of initial and reversible capacity respectively at 0.1 A g<sup>-1</sup> of current density after 200 cycles with stable cyclic performance.</li> </ul>	[123]
Planetary ball milling	Ball milling was carried out with stainless steel balls of 5 mm in diameter with speed of 500 rpm for 360 minutes' duration. Water used as medium for preparing the MoS <sub>2</sub> and graphene.	Sodium-ion batteries	<ul style="list-style-type: none"> <li>➤ Hybrid material from molybdenum sulfide (MoS<sub>2</sub>) and graphene nanosheets was prepared by ball milling and exfoliation method using commercial MoS<sub>2</sub> and graphite precursors</li> <li>➤ The prepared hybrid exhibited higher rate capability of 75 C at 50 A g<sup>-1</sup> current density with 201 mA h g<sup>-1</sup> of reversible stable capacity</li> <li>➤ After 250 cycles, material showed the 95% retention capacity at current density of 0.3 A g<sup>-1</sup>.</li> </ul>	[124]

Table 2. Cont.

Type of Ball Milling	Specification	Battery/Supercapacitor	Highlights	Ref.
Planetary ball milling	La <sub>0.6</sub> Sr <sub>0.4</sub> CoO <sub>3-δ</sub> (LSC) perovskite material was ball milled at different time interval after synthesis it by Pechini method and 1000 °C calcination treatment. Zirconia balls were used to perform ball milling with milling speed of 400 rpm for time duration of 12, 24, 36 and 48 h in presence of ethanol	Lithium air battery	<ul style="list-style-type: none"> <li>➤ The effect of different milling time on structural and electrochemical properties of LSC perovskite synthesized at 1000 °C was studied</li> <li>➤ As the milling time increases the particle size decreases with increasing the surface area, after certain time interval it reverses (particle size increase due to aggregation of particles)</li> <li>➤ The ball milled perovskite showed better electro catalytic activity than the non-ball milled perovskite in terms of oxygen reduction and evolution reactions.</li> </ul>	[125]
Ball Milling	2 h of ball milling with stainless steel balls was performed on Li <sub>1.02</sub> Ni <sub>0.4</sub> Co <sub>0.2</sub> Mn <sub>0.4</sub> O <sub>2</sub> material prepared by the sol-gel method using citric acid followed by the decomposition and sintering process.	Rechargeable lithium batteries	<ul style="list-style-type: none"> <li>➤ The cathode material for the electrochemical application is prepared by ball milled layered Li<sub>1.02</sub>Ni<sub>0.4</sub>Co<sub>0.2</sub>Mn<sub>0.4</sub>O<sub>2</sub> material with carbon</li> <li>➤ The electrochemical performance of ball milled sample and manually ground sample are analyzed</li> <li>➤ First cycle discharge capacity for ball milled (BM) and manually ground (MG) sample was measured as 167 and 156 mA h g<sup>-1</sup> resp. Retention capacity of 87 and 75% was measured for BM and MG sample at 8C after 50 number of cycles.</li> </ul>	[126]
Plasma assisted ball milling (P-milling)	50:1 ratio of ball (stainless steel) to powder ratio in argon atmosphere used in milling. The cylinder of ball milled vibrated with 16 Hz frequency. 60 kHz discharge frequency with 1.5 A current is applied during milling process.	Potassium-ion batteries (PIBs)	<ul style="list-style-type: none"> <li>➤ Different composites of selenium, red phosphate, and carbon (Se/P/C) with different molar ratios and milling time was prepared</li> <li>➤ Se-P composite with carbon coating shown better performance as anode material in PIBs</li> <li>➤ Molar ratio of 1:2 for Se: P (C-coating) with P-ball milling for 30 h exhibits 634 mA h g<sup>-1</sup> of reversible capacity at 0.05 A g<sup>-1</sup> current density also showed 248.6 mA h g<sup>-1</sup> of rate capability at 1 A g<sup>-1</sup> of current density.</li> </ul>	[127]
Ball Milling	Lithium sulfate (Li <sub>2</sub> SO <sub>4</sub> ) and Sodium sulfate (Na <sub>2</sub> SO <sub>4</sub> ) salts were ball milled using stainless steel balls. 1:6 ball to powder ratio with different milling time (2, 4, 8 h) was used.	Thermal energy storage	<ul style="list-style-type: none"> <li>➤ Lithium sulfate (LS)-Sodium sulfate (NS) composite used for thermal energy storage (TES) application at 450–550 °C temperature.</li> <li>➤ The theoretical performance of TES was determined by the analysis of theoretical parameters</li> <li>➤ LS/NS composite with 79:21 and 50:50 stoichiometric ratio exhibited 270 J g<sup>-1</sup> and 318 J g<sup>-1</sup> of theoretical enthalpy transformation value resp. and enthalpy value of 185 J g<sup>-1</sup> and 160 J g<sup>-1</sup> respectively.</li> </ul>	[128]

Table 2. Cont.

Type of Ball Milling	Specification	Battery/Supercapacitor	Highlights	Ref.
Dielectric barrier discharge plasma assisted milling (P-milling)	Commercial germanium (Ge) and graphite (C) powders in 1:1 mass ratio, steel ball: powder ratio of 50:1 in argon atmosphere	Lithium-ion batteries	<ul style="list-style-type: none"> <li>➤ The nanocomposite prepared by Ge NPs (150 nm) wrapped with few-layer graphene sheets (10 layers) (Ge@FLG)</li> <li>➤ Ge@FLG composite anode showed nearly 90 <math>\Omega</math> of charge transfer resistance</li> <li>➤ Ge@FLG composite exhibited 846.3 mA h g<sup>-1</sup> of capacity with 86% of retention.</li> </ul>	[40]
Dielectric barrier discharge plasma assisted milling (P-milling)	Sn powder and graphite in 1:1 ratio, ball to powder in 50:1 weight ratio used in argon atmosphere	Lithium-ion batteries	<ul style="list-style-type: none"> <li>➤ Electrochemical performance of plasma assisted Sn-C composite (anode material) milled for 10 h showed 61.8% of initial coulombic efficiency and 818.7 mA h g<sup>-1</sup> of initial capacity</li> <li>➤ The retention capacity with 385 mA h g<sup>-1</sup> supported up to 40 cycles</li> </ul>	[129]

Thus, ball milling is a versatile technique that can handle various elements, gives an easy approach to tailor the composition of nanocomposites, and produces defect-generated nanomaterials that aid in boosting the performance of devices as tabulated in Table 2.

Hydrogen is a clean fuel. The present hydrogen economy has targeted hydrogen production and storage as key challenges. If hydrogen can be successfully stored within materials, then hydrogen on release can function as a clean fuel. In 2005, Imamura et al. [116] reported the hydrogen storage ability of the nano sized magnesium crystallites and  $\text{MgH}_2$  (as received) ball milled with and without benzene (organic additives). The  $\text{H}_2$  storage ability was tested by doping aluminum and nickel in  $\text{MgH}_2$  sample. The hydrogen storage capacity of ball milled samples showed that the as-received  $\text{MgH}_2$  milled with benzene > milled  $\text{MgH}_2$  > Mg milled with benzene > milled Mg. Ball milled  $\text{MgH}_2$  sample further doped with 1 at.%, and 2.9 at.% Al and Ni, respectively, in benzene showed the satisfactory hydrogen storage and hydriding/dehydriding performance. The maximum reversible hydrogen absorption capacity of 7.3 wt.% was achieved by 1 at.% Al-doped sample than Ni doped sample in  $\text{H}_2$  atmosphere at 0.1 MPa pressure. A composite of nano silicon and graphene nanosheets (Nano-Si/GNs) prepared by discharged plasma assisted milling was employed as anode of lithium-ion batteries. The synergistic effect by fast heating discharge plasma and impact of milling led to the formation of nanostructure composite. In this composite, nano size silicon particles were homogeneously embedded in graphene nanosheets resulting in the formation of plenty of nanosized free spaces. This porosity demonstrated improvement in the electronic conductivity, capability, and cycling stability with  $976 \text{ mA h g}^{-1}$  at current density of  $50 \text{ mA g}^{-1}$  by 20 h P-milled composite. In another study, nickel oxide and reduced graphene oxide (NiO/rGO) nanocomposite was produced by one step ball milling method. The redox reaction between graphene oxide and nickel led to strong bond formation between them. The nanocomposite exhibited the electrochemical performance with  $590 \text{ F/g}$  of specific capacitance at  $1 \text{ A g}^{-1}$  of current density and 88% of retention capability at  $15 \text{ A g}^{-1}$  rate. It also exhibited 100% retention after 1000 cycles of charge and discharge. Graphene oxide has been used in few other studies too. Composites of  $\text{MoS}_2/\text{rGO}$  were used for electrochemical measurements in lithium-ion batteries and supercapacitors by Ji et al. [119]. The interlayers formation of 2D material, enormous active reactive sites, dispersion of  $\text{MoS}_2$  nanosheets in to rGO surface and synergistic effect between  $\text{MoS}_2$  and rGO in the composite showed negligible discharge capacity decay of  $0.2 \text{ A g}^{-1}$  after 100 cycles and  $4 \text{ A g}^{-1}$  after 5000 cycles for lithium-ion batteries and supercapacitors, respectively. In another study, anode material prepared by the composite of  $\text{MoS}_2/\text{graphene}$  by Sun et al. showed 95% of retention capacity with a better cycling stability after 250 cycles at current density of  $0.3 \text{ A g}^{-1}$  for the sodium-ion batteries. The density functional theory (DFT) calculation revealed the possibility of activation of functional groups in the  $\text{MoS}_2/\text{graphene}$  composite. The heterostructures with low degree defects and oxygen residual in graphene improves the conductivity of electrons in composite material and depletion of  $\text{Na}^+$  diffusion barrier. The performance of the composite material with few-layered niobium diselenide ( $\text{NbSe}_2$ ) and graphene synthesized via wet ball milling method (WBMNG) reported by the Nguyen et al. [123]. The anode material by composite showed  $1142 \text{ mA h g}^{-1}$  of initial capacity and  $1000 \text{ mA h g}^{-1}$  of reversible capacity at  $0.1 \text{ A g}^{-1}$  of current density after 200 cycles in lithium-ion battery. The thin layered graphene with smaller  $\text{NbSe}_2$  particles dispersed over it showed an increase in the surface area of the composite material. It also provided an effective electron/ion transport pathway to increase the rate of current in anode material. The layered structure may be responsible for excessive storage capacity. All these properties result in satisfactory electrochemical performance of the WBMNG anode material.

The novel structure of N-graphene by performing one step ball milling method by using (calcium carbide)  $\text{CaC}_2$  and pyrazine with absolute ethanol reported by Ding et al. [123] showed maximum capacitance of  $235 \text{ F g}^{-1}$  of at  $1 \text{ A g}^{-1}$  of current density and 87% of retention capacitance after 3000 cycles of charge and discharge cycles at  $6 \text{ A g}^{-1}$  current density. In this work, Pyrazine was used as nitrogen precursor. Nitrogen heteroatomic defects

and large surface area fast electron transportation improved electrochemical performance of N-graphene.

The properties of layered structured materials with ion conduction studied by the Pflügl et al. [9] showed an improved ionic conductivity of the electrode material up to  $7 \times 10^{-4} \text{ Scm}^{-1}$  by layered-structured materials prepared by the high energy ball milling technique. The effect of annealing the precursor at low temperature led to phase transition of material with increased defects and disorders resulting in good energy storage capabilities. In another work electrochemical performance of the ball milled (BM) and manually ground (MG) layered  $\text{Li}_{1.02}\text{Ni}_{0.4}\text{Co}_{0.2}\text{Mn}_{0.4}\text{O}_2$  material with carbon powder was investigated by Santhanam et al. They reported that the BM sample exhibited better electrochemical performance than the MG sample. The retention capacity was calculated to be 87 and 75% for BM and MG sample respectively at 8C. The conductivity of the layered oxide material was enhanced by adding the carbon powder. The ball milling method leads to a reduction in the contact resistance between layered oxide material and carbon results in increased conductivity of lithium ions and improves the performance of battery.

Anode material prepared by Si powder and carbon coating reported by Nzabimana et al. [8] was used in lithium-ion batteries. The uniform layer (4.5 nm) of carbon coated on porous silicon prepared by milling process of 2 h showed 1016.1 and 834.1  $\text{mA h g}^{-1}$  of reversible capacities at 1000 and 2000  $\text{mA g}^{-1}$  of current densities, respectively, over 200 cycles. It showed 99.5% of coulombic efficiency with stable cycling performance. Theoretically, Si has the highest capacity compared to the graphite-based electrodes, but structural degradation and decaying the electrode capacity with cycling performances limit its uses in practical applications. High energy ball milling with etching process improves the structural and morphological properties of precursor with reducing the particle size and increasing the surface area. The milling time has a powerful impact on crystallinity, morphology, and electrochemical performance of anode materials. Electrode material prepared by Si particles coated with hierarchical carbon and carbon nanofibers investigated by Shen et al. [118]. Particles prepared by different Si sources showed cycling performance up to 1000  $\text{mA h g}^{-1}$  at 2  $\text{A g}^{-1}$  of current density after 1000 cycles. After the cycling performances, Si was well bound with the carbon shell. The energy density of the fuel cell was enhanced by the pairing of a light weighted, free-standing electrode prepared by hierarchical carbon coated Si with  $\text{LiNi}_{0.5}\text{Mn}_{1.5}\text{O}_4$  up to 547  $\text{W h Kg}^{-1}$  over 100 cycles. The fuel cell exhibited 46% of energy density with  $\text{LiNi}_{0.5}\text{Mn}_{1.5}\text{O}_4$  cathode than  $\text{LiCoO}_2$  cathode. Solvothermal ball milling technique used by Yi et al. [120] to synthesize the  $\text{Na}_3\text{V}_2(\text{PO}_4)_2\text{F}_3$  cathode material. The effect of change in pH concentration resulted in a change in morphological structures from 0-D particle to 3-D cube in acidic environment. The short time ball milling was performed to obtain nanosized  $\text{Na}_3\text{V}_2(\text{PO}_4)_2\text{F}_3$  coated with Ketjenblack (KB) (conductive carbon). The  $\text{Na}_3\text{V}_2(\text{PO}_4)_2\text{F}_3$  and KB composite with pH value of 3 exhibited 138  $\text{mA h g}^{-1}$  and 122  $\text{mA h g}^{-1}$  of discharge specific capacity at 0.5C and 40C, respectively. Electrochemical performance of composite materials ( $\text{Fe}_2\text{O}_3$ , MWCNT and PVB) on Ni foam as current collector was reported by Zhang and Zhitomirsky [122]. In this work, the authors prepared three different composites by using maghemite ( $\gamma\text{-Fe}_2\text{O}_3$ ), multi-walled carbon nanotubes (MWCNT), polyvinyl butyral (PVB), and gallocyanine. In composite-1, non-ball milled  $\text{Fe}_2\text{O}_3$  powder was used, while in composite-2, ball milled  $\text{Fe}_2\text{O}_3$  powder was used without the gallocyanine. In composite-3, ball milled  $\text{Fe}_2\text{O}_3$  powder was used with the gallocyanine. Among the other two composites, composite-3 showed capacitance up to 1.53  $\text{F cm}^{-2}$  in 0.5 M sodium sulfate electrolyte. Gallocyanine provided effective co-dispersion for the  $\text{Fe}_2\text{O}_3$  powder and MWCNT. The adequate capacitance led to effective charging and discharging phenomenon favorable for enhancing the capacitive properties in the energy storage devices. The obtained composite material showed mutual interaction between ferromagnetic and capacitive properties, which could be useful in the fabrication of multifunctional devices. The composite of Selenium: Phosphorous: Carbon (Se:P:C) synthesized by a Plasma assisted ball milling (P-milling) method by varying the molar ratios of raw materials and milling time was

reported by Lin et al. [127]. The authors prepared several composites of Se:P:C by P-milling carried out in presence of the 7 mm amplitude and 16 Hz frequency of milling cylinder vibrations. A discharge frequency of 60 kHz with 15 kV voltage and 1.5 A of current was applied. Among the other composites, anode material prepared by the amorphous Se:2P/C@30h composite exhibited better electrochemical performance for Potassium-ion batteries (PIBs) with 634 mA h g<sup>-1</sup> of reversible capacity at 0.05 A g<sup>-1</sup> current density and 248.6 mA h g<sup>-1</sup> of rate capability at 1 A g<sup>-1</sup> of current density. The resultant composite material has lower particle size and reduced the diffusion distance of potassium ion. It also enhanced the conductivity of the active material by preventing the formation of polyse-lenide in the charging and discharging process. The practical performance of the electrode was lower than the theoretical one due to the new incomplete phases due to potassiation. Fabrication of 0.925(K<sub>0.5</sub>Na<sub>0.5</sub>)NbO<sub>3</sub>-0.075Bi(Zn<sub>2/3</sub>(Ta<sub>0.5</sub>Nb<sub>0.5</sub>)<sub>1/3</sub>)O<sub>3</sub> (KNN-BZTN) relaxor ferroelectric ceramic material by Wang et al. [125] via high energy ball milling route showed different morphologies. The effect of high sintering temperature and short relaxation time operated on material in two steps resulted a reduction in the grain size and large number of grain boundaries, effectively enhancing the energy storage performance. The electric breakdown effect was increased from 222 to 317 kV cm<sup>-1</sup> due to large band gap and lower charge carrier concentration properties. The resulting material showed improved energy storage characteristics such as 4.02 J.cm<sup>3</sup> of energy density and 87.4% of energy efficiency.

Besides the electrochemical storage, materials have also been employed for energy storage by other means. The thermal energy storage (TES) capacity of the solid-state Lithium sulfate (LS)-Sodium sulfate (NS) composite, LS/NS composite material synthesized by the ball milled method was investigated by Doppiu et al. [128] composite material was used for TES storage at 450–550 °C temperature. The authors used the Calphad method to study the performance of the TES by analyzing the various theoretical parameters such as heat capacity, free energy, volume expansion, transition temperature, and enthalpies of reactions. The LS/NS composite with 79:21 and 50:50 stoichiometric ratio exhibited 270 J g<sup>-1</sup> and 318 J g<sup>-1</sup> of theoretical enthalpy transformation values respectively and enthalpy value of 185 J g<sup>-1</sup> and 160 J g<sup>-1</sup> respectively. This material could be useful in latent heat storage applications to store heat without loss of temperature. Further, the perovskite material La<sub>0.6</sub>Sr<sub>0.4</sub>CoO<sub>3-δ</sub> (LSC) synthesized by the Pechini method and further calcined at 1000 °C and ball milled at different milling time was studied for the structural and electrochemical performances by Lee et al. [125]. The result showed that as the milling time increased (up to 36 h), the particle size was reduced with increasing the surface area; after a certain milling time (48 h), particles started to aggregate and resulting in increased the particle size. The authors also concluded that the performance of ball milled LSC exhibited superior electrocatalytic activity for oxygen reduction and oxygen evolution reaction (ORR and OER) than the non- ball milled LSC sample. The resulting ball milled sample also showed satisfactory performance for lithium air battery for ORR and OER with high rate of capacity and reversibility.

Plasma milling or P-milling is yet another technique that provides opportunities to synthesize materials with better physical and/or chemical properties. During the P-milling process, electrons and ions of the plasma collide with the reactive precursors with very high speed and transfer their energy to the latter resulting in an increase in the material temperature. If these temperatures are sufficiently high, there is a possibility of material evaporation. The temperature rise may also result in release of thermal stress of the material that, in turn, results in different microstructures of the synthesized material. Lin et al. [130] reported the P-milling method to prepare few layers graphene using different milling media such as germanium oxide, iron oxide, zinc oxide, boron nitride, and tungsten carbide. The relation between number of layers formed and inductive capacity of milling media were investigated. The nanocomposite of germanium (Ge) nanoparticles wrapped with few layered graphene (Ge@FLG) via dielectric barrier discharge plasma (DBDP) assisted method was demonstrated by Ouyang et al. [40]. In this study, nanocomposites with preprocessed (P-milled Ge powder for 5 h and expandable graphite heated at 1000 °C) and DBDP for

10 h in the presence of argon atmosphere exhibited superior anode performance for lithium-ion battery compared to nanocomposites prepared by the same precursors, but without the DBDP and conventional ball milling route. The aggregation of particles started after exceeding the milling time more than 10 h resulted in a decrease in the electrochemical performance. The Ge@FLG nanocomposite showed nearly 90  $\Omega$  lower resistance for charge transportation and capacity of 846.3 mA h g<sup>-1</sup> with 86% of retention rate. In the study by Liu et al. [129], a comparative electrochemical performance of anode material prepared by Sn-C nanocomposite via dielectric barrier discharge plasma assisted milling (DBDP) (PM) and conventional milling (CM) method was reported. A Sn-C composite prepared by PM and CM with 10 h of milling (PM-10 h and CM-10 h, respectively, showed different microstructural composition. While a non-homogenous dispersion of Sn particles in graphite matrix was observed in CM-10 h, the Sn-C composite showed homogenous dispersion of multi-scale Sn particles in graphite matrix via PM-10 Sn-C composite. In plasma state, the charged particles impacted the Sn powder surface with high speed and high energy, resulting in local temperature rise followed by release of the thermal stress. The expansion resulting from the release of thermal stress was uniformly distributed and observed to be homogeneously embedded in graphite matrix. This technique showed that the graphite layers were not damaged as in the case of CM. Coulombic efficiency and capacity at initial stage was observed to be 61.8% and 818.7 mA h g<sup>-1</sup> in PM-10 h composite while 47.9% and 727.4 mA h g<sup>-1</sup> observed in CM-10 h composite. Thus, the PM-10 h composite exhibited superior electrochemical performance than the CM-10 h composite. The required milling time is much shorter in the P-milling process than other milling techniques. Therefore, the P-milling route has significant advantages in synthesizing the material with nano scale and, particularly, resulting in different microstructures due to high chemical reactivity, large surface area, and low temperature operation. The Mg-based hydrogen (H<sub>2</sub>) storage materials and group IV-A elements synthesized by the P-milling method were reported to exhibit remarkable performance as energy storage materials [131].

In another study, a nanocomposite of carbon quantum dots and cobalt sulfide (CQDs/CoS<sub>2</sub>) prepared by the ball milling assisted hydrothermal route reported by Arsalani et al. [132]. In this study, CQDs were prepared by the microwave radiation assisted method. The nanocomposite with highly porous morphology with surface attached CQDs provides a large surface area, extra ion storage spaces, and fast ion transportation pathways may promote to enhance the supercapacitor performance. The electrochemical characteristics of CQDs/CoS<sub>2</sub> nanocomposite and pure CoS<sub>2</sub> (without decoration of CQDs) were tested by the cyclic voltammetry (CV), galvanostatic charge–discharge (GCD), and electrochemical impedance spectroscopy (EIS) studies. CQDs/CoS<sub>2</sub> nanocomposite exhibited superior electrochemical performance than the pure CoS<sub>2</sub> material. The nanocomposite showed a specific capacity of 808 F g<sup>-1</sup> at 1 A g<sup>-1</sup> current density.

## 6. Conclusions

Though there are very recent publications on the reviews of mechanical alloying, basic principles to its applications [133–135], this current review is focused towards deploying ball milled materials and nanocomposite systems for energy storage applications, especially electrochemical and hydrogen storage. This review is also aimed on the recent developments on the synthesis of nanocomposites using the simplest top-down approach, mechanochemical milling, and the related aspects of the interfacial interactions. Milling constraints include time duration of milling, ball size, the ball to sample content proportion, rotation speed, and energy that took part in a vital part of the structure-property relationships and composite interactions. Milled nanocomposites are being used in different structural applications for their higher performance rate and throughput. The synthesis of different nanocomposites (magnetic and non-magnetic metallic systems, polymeric systems, and ceramic systems) and the effect of various parameters on the mill-ability of nanocomposites are discussed. A detailed review of these ball milled materials and their usage in energy storage applications are detailed at the very end of the review.

There is an increasing interest among the materials research community in nanocomposite synthesis via the ball milling method. Simple, cost-effectiveness, and scalability make this top-down route very attractive. If the optimization parameters are properly controlled, it is possible to synthesize a wide variety of nanocomposite materials (polymeric, ceramic, metallic, etc.) with desired size and shape. Researchers integrated their investigations on the impact of different milling factors especially the energy dose and energy intensity on the morphological, physico-chemical, and mechanical properties. The nanocomposite exhibits good dispersion of nanofillers with good interfacial adhesion and also could absorb the load stress, which improves the overall mechanical properties. The ultra-high thermal conductivity should be investigated in the future for ball milled nanocomposite as it is crucial for thermal management. Dry milling at medium energy and wet milling at high energy attributes to an effective method for embedding the nanofiller into the matrix. According to the applications, the right compositions of nanofiller and the matrix should be chosen. The ball milled anode and cathode materials are applicable for large-scale production with better performance. These kinds of metal hydride nanocomposite could be utilized as a hydrogen storage material, as they possess superior hydrogen ions that could be transferred easily through the proton exchange membranes (PEM) in fuel cells. The technological challenges associated with the innovative utilization of milled nanocomposites in advanced applications still to be resolved.

## 7. Future Scope and Outlook

The advances and modifications in the ball milling method attract researchers to synthesize novel functional materials and composites with wide range of possibilities by merely changing the milling parameters and obtaining different morphologies in the materials. The ball milled materials show satisfactory performances in the electrochemical studies and energy storage devices due to smaller particle size, large surface area, huge number of active sites and defects that result in enhancing the surface properties of the materials such as reactivity, functionalization possibility with foreign atoms, etc. The defected and fractured material that results after milling is indeed a collection of a host of sites that can favor functionalization by catalytic species. Thus, energy storage will be more efficient for a given amount of active electrode material.

Theoretical investigations about reaction processes and optimization of experimental results need to be explored more for better functionalization and structural studies. Pan milling, plasma assisted milling techniques should be explored to achieve the materials with novel properties.

Mechanical milling has the potential to expand the market for high-quality, high-throughput nanocomposites. To increase the viability and reproducibility of mechanically alloyed nanocomposites, additional research on condition optimization would be quite interesting. Increases in feedstock temperature, particularly when utilizing high-energy ball mills, must be taken into consideration because they have an impact on the reactivity of materials that are sensitive to temperature (plastics and nanocrystalline powders). Research should also be performed to investigate whether mills can be used to process chemically altered nanoparticles. To optimize interactions and achieve uniform dispersion, it is required to study strategies to better incorporate nanofillers into the primary matrix of the composite, which, in turn, necessitates optimization at many levels in order to achieve the desired properties. To explain the prospective uses of ball milled nanocomposites, extensive research insights might be obtained.

**Author Contributions:** Conceptualization, J.J., A.K., S.S.; methodology, A.K. and A.T.; data analysis, J.J., A.K. and A.T.; applications, V.K. and R.N.; literature, A.K., V.K., R.N. and S.S.; writing—original draft preparation, J.J., A.K., A.T. and R.N.; writing—review and editing, A.K. and S.S.; visualization, J.J., A.K. and A.T.; supervision, A.K. and S.S. All authors have read and agreed to the published version of the manuscript.

**Funding:** This research received no external funding.

**Institutional Review Board Statement:** Not applicable.

**Informed Consent Statement:** Not applicable.

**Data Availability Statement:** Not applicable.

**Acknowledgments:** Authors gratefully acknowledge their respective institutions for the support and encouragement to carry out the research as part of this review study.

**Conflicts of Interest:** The authors declare no conflict of interest.

## References

1. Benjamin, J.S. Dispersion strengthened superalloys by mechanical alloying. *Metall. Trans.* **1970**, *1*, 2943–2951. [\[CrossRef\]](#)
2. Koch, C.C.; Ovid'ko, I.A.; Seal, S.; Veprek, S. *Structural Nanocrystalline Materials Fundamentals and Applications*; Cambridge University Press: New York, NY, USA, 2007; pp. 29–36.
3. Boldyreva, E. Mechanochemistry of inorganic and organic systems: What is similar, what is different? *Chem. Soc. Rev.* **2013**, *42*, 7719–7738. [\[CrossRef\]](#)
4. Suryanarayana, C. Mechanical alloying and milling. *Prog. Mater. Sci.* **2001**, *46*, 1–184. [\[CrossRef\]](#)
5. Suryanarayana, C. *Mechanical Alloying and Milling*, 1st ed.; CRC Press: Boca Raton, FL, USA; Marcel Dekker Inc.: New York, NY, USA, 2004; 488p. [\[CrossRef\]](#)
6. Baláž, P.; Achimovičová, M.; Baláž, M.; Billik, P.; Cherkezova-Zheleva, Z.; Criado, J.M.; Delogu, F.; Dutková, E.; Gaffet, E.; Gotor, F.J.; et al. Hallmarks of mechanochemistry: From nanoparticles to technology. *Chem. Soc. Rev.* **2013**, *42*, 7571–7637. [\[CrossRef\]](#)
7. Ding, W.; Sun, M.; Gao, B.; Liu, W.; Ding, Z.; Anandan, S. A ball-milling synthesis of N-graphyne with controllable nitrogen doping sites for efficient electrocatalytic oxygen evolution and supercapacitors. *Dalton Trans.* **2020**, *49*, 10958–10969. [\[CrossRef\]](#)
8. Nzabahimana, J.; Chang, P.; Hu, X. Porous carbon-coated ball-milled silicon as high-performance anodes for lithium-ion batteries. *J. Mater. Sci.* **2018**, *54*, 4798–4810. [\[CrossRef\]](#)
9. Preishuber-Pflügl, F.; Epp, V.; Nakhal, S.; Lerch, M.; Wilkening, M. Defect-enhanced F<sup>-</sup> ion conductivity in layer-structured nanocrystalline BaSnF<sub>4</sub> prepared by high-energy ball milling combined with soft annealing. *Phys. Status Solidi C* **2015**, *12*, 10–14. [\[CrossRef\]](#)
10. Prabakaran, S.; Rajan, M. Biosynthesis of nanoparticles and their roles in numerous areas. *Compr. Anal. Chem.* **2021**, *94*, 1–47.
11. Tanna, A.R.; Srinivasan, S.S.; Joshi, H.H. Enhancement in magnetoelectric properties of lead-free multiferroic composite through high-energy mechanical milling. *J. Mater. Sci. Mater. Electron.* **2020**, *31*, 9306–9320. [\[CrossRef\]](#)
12. Li, F.; Wan, Y.; Chen, J.; Hu, X.; Tsang, D.C.; Wang, H.; Gao, B. Novel ball-milled biochar-vermiculite nanocomposites effectively adsorb aqueous As(V). *Chemosphere* **2020**, *260*, 127566. [\[CrossRef\]](#)
13. Kamrani, S.; Penther, D.; Ghasemi, A.; Riedel, R.; Fleck, C. Microstructural characterization of Mg-SiC nanocomposite synthesized by high energy ball milling. *Adv. Powder Technol.* **2018**, *29*, 1742–1748. [\[CrossRef\]](#)
14. Ni, J.; Li, J.; Luo, W.; Han, Q.; Yin, Y.; Jia, Z.; Huang, B.; Hu, C.; Xu, Z. Microstructure and properties of in-situ TiC reinforced copper nanocomposites fabricated via long-term ball milling and hot pressing. *J. Alloys Compd.* **2018**, *755*, 24–28. [\[CrossRef\]](#)
15. Wagih, A.; Fathy, A.; Kabeel, A. Optimum milling parameters for production of highly uniform metal-matrix nanocomposites with improved mechanical properties. *Adv. Powder Technol.* **2018**, *29*, 2527–2537. [\[CrossRef\]](#)
16. Saheb, N.; Khan, M.S.; Hakeem, A.S. Effect of Processing on Mechanically Alloyed and Spark Plasma Sintered Al-Al<sub>2</sub>O<sub>3</sub> Nanocomposites. *J. Nanomater.* **2015**, *2015*, 377. [\[CrossRef\]](#)
17. AlMangour, B.; Grzesiak, D.; Yang, J.M. In situ formation of TiC-particle-reinforced stainless steel matrix nanocomposites during ball milling: Feedstock powder preparation for selective laser melting at various energy densities. *Powder Technol.* **2018**, *326*, 467–478. [\[CrossRef\]](#)
18. Jazi, E.H.; Borhani, G.; Farsani, R.E. Preparation of Al-Fe/TiB<sub>2</sub> nanocomposite powder by ball milling and subsequent heat treatment. *Micro Nano Lett.* **2012**, *7*, 448–452. [\[CrossRef\]](#)
19. Xu, W.; Galano, M.; Audebert, F. Nanoquasicrystalline Al-Fe-Cr-Ti alloy matrix/ $\gamma$ -Al<sub>2</sub>O<sub>3</sub> nanocomposite powders: The effect of the ball milling process. *J. Alloys Compd.* **2017**, *701*, 342–349. [\[CrossRef\]](#)
20. Gass, J.; Srikanth, H.; Kislov, N.; Srinivasan, S.S.; Emirov, Y. Magnetization and magnetocaloric effect in ball-milled zinc ferrite powder. *J. Appl. Phys.* **2008**, *103*, 23–25. [\[CrossRef\]](#)
21. Delogu, F.; Gorrasi, G.; Sorrentino, A. Progress in Materials Science Fabrication of polymer nanocomposites via ball milling: Present status and future perspectives. *Prog. Mater. Sci.* **2017**, *86*, 75–126.
22. Puchy, V.; Hvizdos, P.; Dusza, J.; Kovac, F.; Inam, F.; Reece, M. Wear resistance of Al<sub>2</sub>O<sub>3</sub>-CNT ceramic nanocomposites at room and high temperatures. *Ceram. Int.* **2013**, *39*, 5821–5826. [\[CrossRef\]](#)
23. Hannora, A.E.; Ataya, S. Structure and compression strength of hydroxyapatite/titania nanocomposites formed by high energy ball milling. *J. Alloys Compd.* **2016**, *658*, 222–233. [\[CrossRef\]](#)
24. Kumar, A.; Banerjee, U.; Chowrasia, M.K.; Shekhar, H.; Banerjee, M.K. Effect of MWCNT Content on the Structure and Properties of Spark Plasma-Sintered Iron-MWCNT Composites Synthesized by High-Energy Ball Milling. *J. Mater. Eng. Perform.* **2019**, *28*, 2983–3000. [\[CrossRef\]](#)

25. Araujo, E.G.; Neto, R.M.L.; Pillis, M.F.; Filho, F.A. High Energy Ball Mill Processing. Available online: [https://www.ipen.br/biblioteca/cd/ptech/2001/5\\_03.PDF](https://www.ipen.br/biblioteca/cd/ptech/2001/5_03.PDF) (accessed on 12 September 2022).
26. El-Eskandarany, M.S. Controlling the powder milling process. In *Mechanical Alloying*, 2nd ed.; Elsevier Publications: New York, NY, USA, 2015; pp. 48–83. ISBN 9781455777525.
27. Anand, K.; Varghese, S.; Kurian, T. Preparation of ultra-fine dispersions of zinc oxide by simple ball-milling: Optimization of process parameters. *Powder Technol.* **2015**, *271*, 187–192. [[CrossRef](#)]
28. Piras, C.C.; Fernández-Prieto, S.; De Borggraeve, W.M. Ball milling: A green technology for the preparation and functionalisation of nanocellulose derivatives. *Nanoscale Adv.* **2019**, *1*, 937–947. [[CrossRef](#)]
29. Wei, X.; Wang, X.; Gao, B.; Zou, W.; Dong, L. Facile Ball-Milling Synthesis of CuO/Biochar Nanocomposites for Efficient Removal of Reactive Red 120. *ACS Omega* **2020**, *5*, 5748–5755. [[CrossRef](#)]
30. Gorrasí, G.; Sorrentino, A. Mechanical milling as a technology to produce structural and functional bio-nanocomposites. *Green Chem.* **2015**, *17*, 2610–2625. [[CrossRef](#)]
31. Krause, B.; Villmow, T.; Boldt, R.; Mende, M.; Petzold, G.; Pötschke, P. Influence of dry grinding in a ball mill on the length of multiwalled carbon nanotubes and their dispersion and percolation behaviour in melt mixed polycarbonate composites. *Compos. Sci. Technol.* **2011**, *71*, 1145–1153. [[CrossRef](#)]
32. Verma, R.; Rathod, M.; Goyal, R. Effect of milling parameters on EMI shielding of the PES/MWCNT nanocomposites. *Mater. Today Proc.* **2021**, *43*, 3169–3172. [[CrossRef](#)]
33. Restivo, J.; Orge, C.A.; Santos, A.S.G.; Soares, O.S.G.; Pereira, M.F.R. Nano- and macro-structured cerium oxide–Carbon nanotubes composites for the catalytic ozonation of organic pollutants in water. *Catal. Today* **2022**, *384–386*, 187–196. [[CrossRef](#)]
34. Bor, A.; Jargalsaikhan, B.; Lee, J.; Choi, H. Effect of Different Milling Media for Surface Coating on the Copper Powder Using Two Kinds of Ball Mills with Discrete Element Method Simulation. *Coatings* **2020**, *10*, 898. [[CrossRef](#)]
35. Zhang, Z.; Shang, H.; Zhang, X.; Liu, C.; Li, S.; Wen, Z.; Ji, S.; Sun, J. Enhancing the Electrochemical Performances by Wet Ball Milling to Introduce Structural Water into an Electrolytic MnO<sub>2</sub>/Graphite Nanocomposite Cathode for Zinc-Ion Batteries. *ACS Appl. Energy Mater.* **2021**, *4*, 5113–5122. [[CrossRef](#)]
36. Liu, Y.; Zeng, M.; Lu, Z.; Zhu, M. Applications of Plasma Milling in Materials Preparation. *Mater. Rep.* **2022**, *36*, 20120251–20120259. [[CrossRef](#)]
37. Liu, Z.-J.; Yang, D.-Z.; Wang, W.-C.; Dai, L.-Y.; Shaibo, J. Effect of Different Precursors on Synthesized AlN by Plasma-Assisted Ball Milling. *Mater. Manuf. Process.* **2016**, *31*, 1583–1588. [[CrossRef](#)]
38. Sun, W.; Hu, R.; Liu, H.; Zeng, M.; Yang, L.; Wang, H.; Zhu, M. Embedding nano-silicon in graphene nanosheets by plasma assisted milling for high capacity anode materials in lithium ion batteries. *J. Power Sources* **2014**, *268*, 610–618. [[CrossRef](#)]
39. Yang, S.; Wang, H.; Ouyang, L.; Liu, J.; Zhu, M. Improvement in the Electrochemical Lithium Storage Performance of MgH<sub>2</sub>. *Inorganics* **2017**, *6*, 2. [[CrossRef](#)]
40. Ouyang, L.; Guo, L.; Cai, W.; Ye, J.; Hu, R.; Liu, J.; Yang, L.; Zhu, M. Facile synthesis of Ge@FLG composites by plasma assisted ball milling for lithium ion battery anodes. *J. Mater. Chem. A* **2014**, *2*, 11280–11285. [[CrossRef](#)]
41. Baghani, M.; Aliofkhaezrai, M.; Poursalehi, R. Microwave-assisted Sintering of Fe-Al<sub>2</sub>O<sub>3</sub> Nanocomposites: Study of Corrosion and Wear Properties. *Procedia Mater. Sci.* **2015**, *11*, 689–694. [[CrossRef](#)]
42. Ning, R.; Chen, D.; Zhang, Q.; Bian, Z.; Dai, H.; Zhang, C. Surface modification of titanium hydride with epoxy resin via microwave-assisted ball milling. *Appl. Surf. Sci.* **2014**, *316*, 632–636. [[CrossRef](#)]
43. Ashwath, P.; Xavier, M.A.; Rajendran, R.; Batako, A.D.L.; Jeyapandiarajan, P.; Joel, J. Microwave-assisted T6 heat treating of aluminium alloy-Al<sub>2</sub>O<sub>3</sub> nanocomposites. *MRS Commun.* **2022**, *12*, 245–249. [[CrossRef](#)]
44. Zhao, Z. Microwave-assisted synthesis of vanadium and chromium carbides nanocomposite and its effect on properties of WC-8Co cemented carbides. *Scr. Mater.* **2016**, *120*, 103–106. [[CrossRef](#)]
45. Calka, A.; Wexler, D. Mechanical milling assisted by electrical discharge. *Nature* **2002**, *419*, 147–151. [[CrossRef](#)]
46. Xu, M.; Li, C.; Kurniawan, R.; Park, G.; Chen, J.; Ko, T.J. Study on surface integrity of titanium alloy machined by electrical discharge-assisted milling. *J. Mater. Process. Technol.* **2021**, *299*, 117334. [[CrossRef](#)]
47. Poudyal, N.; Altuncevahir, B.; Chakka, V.; Chen, K.; Black, T.D.; Liu, J.P.; Ding, Y.; Wang, Z.L. Field-ball milling induced anisotropy in magnetic particles. *J. Phys. D Appl. Phys.* **2004**, *37*, L45–L48. [[CrossRef](#)]
48. Wang, D.; Li, X.; Chang, Y.; Zhu, M.; Li, W.; Qi, M. Anisotropic Sm<sub>2</sub>Co<sub>17</sub> nano-flakes produced by surfactant and magnetic field assisted high energy ball milling. *J. Rare Earths* **2013**, *31*, 366–369. [[CrossRef](#)]
49. Chelvane, J.A.; Palit, M.; Basumatary, H.; Pandian, S. Magnetic properties of TbFe<sub>2</sub> particles prepared by magnetic field assisted ball milling. *J. Magn. Magn. Mater.* **2013**, *343*, 144–148. [[CrossRef](#)]
50. Altuncevahir, B.; Poudyal, N.; Chakka, V.M.; Chen, K.H.; Black, T.D.; Liu, T.D. Effect of magnetic field on ball milled hard magnetic particles. In Proceedings of the American Physical Society, March Meeting 2004, Montreal, QC, Canada, 22–26 March 2004.
51. Mordyuk, B.; Prokopenko, G. Mechanical alloying of powder materials by ultrasonic milling. *Ultrasonics* **2004**, *42*, 43–46. [[CrossRef](#)]
52. Chen, D.; Liu, H.Y.; Li, L. One-step synthesis of manganese ferrite nanoparticles by ultrasonic wave-assisted ball milling technology. *Mater. Chem. Phys.* **2012**, *134*, 921–924. [[CrossRef](#)]
53. Shi, D.; Yang, M.; Chang, B.; Ai, Z.; Zhang, K.; Shao, Y.; Wang, S.; Wu, Y.; Hao, X. Ultrasonic-Ball Milling: A Novel Strategy to Prepare Large-Size Ultrathin 2D Materials. *Small* **2020**, *16*, e1906734. [[CrossRef](#)]

54. Jiang, S.; Li, X.; Zuo, D.; Wang, H.; Liu, Z.; Xu, R. A comparative study on nano La<sub>2</sub>O<sub>3</sub> suspension treated by ultrasonic and ball milling. *J. Rare Earths* **2012**, *30*, 1116–1122. [[CrossRef](#)]
55. Liang, Z.; Wang, S.; Zhu, K.; Chen, Y.; Wei, F.; Chen, D. Enhancing the tribological properties and corrosion resistance of graphene-based lubricating grease via ultrasonic-assisted ball milling. *Colloids Surf. A Physicochem. Eng. Asp.* **2022**, *633*, 127889. [[CrossRef](#)]
56. Fu, D.; Ma, X.; Chen, D. Degradation of Azo Dye in Wastewater by Ultrasonic Assisted Ball Milling. *J. Hunan Univ. Nat. Sci.* **2017**, *44*, 82–88. [[CrossRef](#)]
57. Atzmon, M. In situ thermal observation of explosive compound-formation reaction during mechanical alloying. *Phys. Rev. Lett.* **1990**, *64*, 487–490. [[CrossRef](#)]
58. Liu, S.-S.; Sun, L.-X.; Zhang, Y.; Xu, F.; Zhang, J.; Chu, H.-L.; Fan, M.-Q.; Zhang, T.; Song, X.-Y.; Grolier, J.-P.E. Effect of ball milling time on the hydrogen storage properties of TiF<sub>3</sub>-doped LiAlH<sub>4</sub>. *Int. J. Hydrogen Energy* **2009**, *34*, 8079–8085. [[CrossRef](#)]
59. Davis, R.M.; McDermott, B.; Koch, C.C. Mechanical alloying of brittle materials. *Met. Trans. A* **1988**, *19*, 2867–2874. [[CrossRef](#)]
60. McDermott, B.; Koch, C. Preparation of beta brass by mechanical alloying of elemental copper and zinc. *Scr. Met.* **1986**, *20*, 669–672. [[CrossRef](#)]
61. Kimura, H.; Kimura, M.Y.; Takada, F. Development of an extremely high energy ball mill for solid state amorphizing transformation. *J. Less Common Met.* **1988**, *140*, 113–118. [[CrossRef](#)]
62. Cabañas-Moreno, J.; López, V.; Calderón, H.; Rendón-Angeles, J. Mechanical alloying of Co<sub>2</sub>Cu powder mixtures. *Scr. Met. Mater.* **1993**, *28*, 645–650. [[CrossRef](#)]
63. Koch, C.C.; Cavin, O.B.; McKamey, C.G.; Scarbrough, J.O. Preparation of amorphous Ni<sub>60</sub>Nb<sub>40</sub> by mechanical alloying. *Appl. Phys. Lett.* **1983**, *43*, 1017–1019. [[CrossRef](#)]
64. Lu, L.; Lai, M.O. *Mechanical Alloying*; Kluwer Academic Publishers: Norwell, MA, USA, 1998; 276p, ISBN 9780792380665.
65. Aymard, L.; Dumont, B.; Viau, G. Production of CoNi alloys by mechanical-alloying. *J. Alloys Compd.* **1996**, *242*, 108–113. [[CrossRef](#)]
66. Li, B.; Li, A.; Zhao, S.; Meyers, M. Amorphization by mechanical deformation. *Mater. Sci. Eng. R Rep.* **2022**, *149*, 100673. [[CrossRef](#)]
67. Shen, F.; Sun, S.; Yang, J.; Qiu, M.; Qi, X. Coupled pretreatment with liquid nitrogen and ball milling for enhanced cellulose hydrolysis in water. *ACS Omega* **2019**, *4*, 11756–11759. [[CrossRef](#)] [[PubMed](#)]
68. Chen, Y.; Halstead, T.; Williams, J. Influence of milling temperature and atmosphere on the synthesis of iron nitrides by ball milling. *Mater. Sci. Eng. A* **1996**, *206*, 24–29. [[CrossRef](#)]
69. Sugimoto, S.; Niwa, T.; Nakanishi, Y.; Danjo, K. Development of a novel ultra cryo-milling technique for a poorly water-soluble drug using dry ice beads and liquid nitrogen. *Int. J. Pharm.* **2012**, *426*, 162–169. [[CrossRef](#)]
70. Riktor, M.D.; Deledda, S.; Herrich, M.; Gutfleisch, O.; Fjellvåg, H.; Hauback, B.C. Hydride formation in ball-milled and cryomilled Mg–Fe powder mixtures. *Mater. Sci. Eng. B* **2009**, *158*, 19–25. [[CrossRef](#)]
71. Ponhan, K.; Tassenberg, K.; Weston, D.; Nicholls, K.G.; Thornton, R. Effect of SiC nanoparticle content and milling time on the microstructural characteristics and properties of Mg–SiC nanocomposites synthesized with powder metallurgy incorporating high-energy ball milling. *Ceram. Int.* **2020**, *46*, 26956–26969. [[CrossRef](#)]
72. Jha, P.; Gautam, R.K.; Tyagi, R. Effect of Reinforcement Content and Technological Parameters on the Properties of Cu-4 wt.% Ni–TiC Composites. *J. Mater. Eng. Perform.* **2017**, *26*, 5126–5136. [[CrossRef](#)]
73. Yang, G.; Park, S. Deformation of Single Crystals, Polycrystalline Materials, and Thin Films: A Review. *Materials* **2019**, *12*, 2003. [[CrossRef](#)]
74. Bastwros, M.; Kim, G.-Y.; Zhu, C.; Zhang, K.; Wang, S.; Tang, X.; Wang, X. Effect of ball milling on graphene reinforced Al6061 composite fabricated by semi-solid sintering. *Compos. Part B Eng.* **2014**, *60*, 111–118. [[CrossRef](#)]
75. Aslibeiki, B.; Kameli, P. Structural and magnetic properties of Co/Al<sub>2</sub>O<sub>3</sub> cermet synthesized by mechanical ball milling. *Ceram. Int.* **2020**, *46*, 20116–20121. [[CrossRef](#)]
76. Joshua, K.J.; Sabesh, S.; Vivekanandan, S.; Saravana, S.; Vetri, M. Effect of Ball Milling for AA7068 Metal Powders for Variable Speeds. *Int. J. Adv. Res. Trends Eng. Technol. IJARTET* **2017**, *4*, 23–26.
77. Bor, A.; Ichinkhorloo, B.; Uyanga, B.; Lee, J.; Choi, H. Cu/CNT nanocomposite fabrication with different raw material properties using a planetary ball milling process. *Powder Technol.* **2018**, *323*, 563–573. [[CrossRef](#)]
78. Pramanik, A.; Basak, A.; Dong, Y.; Shankar, S.; Littlefair, G. Milling of Nanoparticles Reinforced Al-Based Metal Matrix Composites. *J. Compos. Sci.* **2018**, *2*, 13. [[CrossRef](#)]
79. Masroor, M.; Sheibani, S.; Ataie, A. Effect of milling energy on preparation of Cu–Cr/CNT hybrid nano-composite by mechanical alloying. *Trans. Nonferrous Met. Soc. China* **2016**, *26*, 1359–1366. [[CrossRef](#)]
80. Bashirom, N.; Ismah, N.; Arif, M. Effect of Milling Speed on the Synthesis of In-Situ Cu-25 Vol. % WC Nanocomposite by Mechanical Alloying. *J. Teknol.* **2012**, *59*, 229–233. [[CrossRef](#)]
81. Anand, K.; Varghese, S.; Kurian, T. Effect of ball size on milling efficiency of zinc oxide dispersions. *Part. Sci. Technol.* **2018**, *36*, 308–311.
82. Anand, K.; Varghese, S.; Kurian, T. Aqueous Dispersions of Latex Compounding Ingredients by Wet Ball Milling: Effect of Ball Size and Milling Time on Dispersion Quality. *Trans. Indian Inst. Met.* **2017**, *70*, 1593–1600. [[CrossRef](#)]
83. Ashwath, P.; Xavior, M.A. The effect of ball milling & reinforcement percentage on sintered samples of aluminium alloy metal matrix composites. *Procedia Eng.* **2014**, *97*, 1027–1032.

84. Kuziora, P.; Wyszyńska, M.; Polanski, M.; Bystrzycki, J. Why the ball to powder ratio (BPR) is insufficient for describing the mechanical ball milling process. *Int. J. Hydrogen Energy* **2014**, *39*, 9883–9887. [[CrossRef](#)]
85. Wu, Z.; Liang, Y.; Fan, Y.; Wang, P.; Du, J.; Zhao, Y.; Fu, E. The ball to powder ratio (BPR) dependent morphology and microstructure of tungsten powder refined by ball milling. *Powder Technol.* **2018**, *339*, 256–263. [[CrossRef](#)]
86. Cagnetta, G.; Huang, J.; Wang, B.; Deng, S.; Yu, G. A comprehensive kinetic model for mechanochemical destruction of persistent organic pollutants. *Chem. Eng. J.* **2016**, *291*, 30–38. [[CrossRef](#)]
87. Kessler, M.; Rinaldi, R. Kinetic energy dose as a unified metric for comparing ball mills in the mechanocatalytic depolymerization of lignocellulose. *Front. Chem.* **2018**, *9*, 816553. [[CrossRef](#)] [[PubMed](#)]
88. Jargalsaikhan, B.; Bor, A.; Lee, J.; Choi, H. Effect of different raw material property for the fabrication on Al/CNT nanocomposite using a ball mill with a discrete element method (DEM) simulation. *Materials* **2019**, *12*, 3291. [[CrossRef](#)]
89. Fathy, A.; Wagih, A.; Abu-Oqail, A. Effect of ZrO<sub>2</sub> content on properties of Cu-ZrO<sub>2</sub> nanocomposites synthesized by optimized high energy ball milling. *Ceram. Int.* **2018**, *45*, 2319–2329. [[CrossRef](#)]
90. Abu-Oqail, A.; Wagih, A.; Fathy, A.; Elkady, O.; Kabeel, A.M. Effect of high energy ball milling on strengthening of Cu-ZrO<sub>2</sub> nanocomposites. *Ceram. Int.* **2019**, *45*, 5866–5875. [[CrossRef](#)]
91. Zawrah, M.F.; Essawy, R.A.; Zayed, H.A.; Fattah, A.H.A.; Taha, M.A. Mechanical alloying, sintering and characterization of Al<sub>2</sub>O<sub>3</sub>-20 wt.%-Cu nanocomposite. *Ceram. Int.* **2014**, *40*, 31–38. [[CrossRef](#)]
92. Lather, S.; Dalal, J.; Gupta, A.; Singh, S.; Singh, D.; Dahiya, S.; Maan, A.; Tripathi, R.; Ohlan, A. PbTiO<sub>3</sub>-Ni<sub>0.5</sub>Co<sub>0.5</sub>Fe<sub>2</sub>O<sub>4</sub> multiferroic nanocomposites: Impact of ball-milling on dielectric, magnetic and ferroelectric properties. *Ceram. Int.* **2018**, *45*, 4957–4963. [[CrossRef](#)]
93. Zhuge, Y.; Li, Y.; Xu, X.; Zhang, D.; Zhang, H.; Liu, W. Morphology and magnetic properties of Sm<sub>2</sub>Co<sub>7</sub>/α-Fe nanocomposite magnets produced by high energy ball milling and spark plasma. *J. Rare Earths* **2021**, *39*, 312–316. [[CrossRef](#)]
94. Su, Y.; Su, H.; Zhu, Y.; Wang, F.; Du, J.; Xia, W.; Yan, A.; Liu, J.P.; Zhang, J. Effects of magnetic field heat treatment on Sm-Co/α-Fe nanocomposite permanent magnetic materials prepared by high energy ball milling. *J. Alloys Compd.* **2015**, *647*, 375–379. [[CrossRef](#)]
95. López, G.P.; Silvetti, S.; Urreta, S.; Carreras, A. Structure and magnetic properties of NiZn ferrite/SiO<sub>2</sub> nanocomposites synthesized by ball milling. *J. Alloys Compd.* **2010**, *505*, 808–813. [[CrossRef](#)]
96. Chen, J.; Wang, F.; Wang, F.; Meng, F.; Zhang, J. Phase structure and magnetic properties of La/Ce substituted nanocomposite SmCo<sub>5</sub>/α-Fe magnets prepared by high energy ball milling and subsequent annealing. *J. Magn. Magn. Mater.* **2021**, *521*, 167534. [[CrossRef](#)]
97. Hashim, U.R.; Jumahat, A. Improved Tensile and Fracture Toughness Properties of Graphene Nanoplatelets Filled Epoxy Polymer via Solvent Compounding Shear Milling Method. *Mater. Res. Express* **2018**, *6*, 025303. [[CrossRef](#)]
98. González-benito, J.; Sánchez, F.A.; Olmos, D.; Martínez-tarifa, J.M.; González-gaitano, G. PVDF/BaTiO<sub>3</sub>/carbon nanotubes ternary nanocomposites prepared by ball milling: Piezo and dielectric responses. *J. Appl. Polym. Sci.* **2019**, *136*, 47788. [[CrossRef](#)]
99. Tanna, A.R.; Joshi, H.H. Effect of high energy mechanical milling on hysteresis and dielectric properties of C<sub>x</sub>Ba<sub>1-x</sub>Zr<sub>x</sub>Ti<sub>1-x</sub>O<sub>3</sub> (x = 0 and 0.1) ferroelectric materials. *Mater. Res. Express* **2018**, *5*, 096302. [[CrossRef](#)]
100. Wu, H.; Zhao, W.; Chen, G. One-Pot in situ Ball Milling Preparation of Polymer/Graphene Nanocomposites. *J. Appl. Polym. Sci.* **2012**, *125*, 3899–3903. [[CrossRef](#)]
101. Li, N.; Niu, M.; Zhang, B.; Zhao, S.; Xiong, S.; Xie, F. Effects of concurrent ball milling and octenyl succinylation on structure and physicochemical properties of starch. *Carbohydr. Polym.* **2017**, *155*, 109–116. [[CrossRef](#)] [[PubMed](#)]
102. Dai, L.; Li, C.; Zhang, J.; Cheng, F. Preparation and characterization of starch nanocrystals combining ball milling with acid hydrolysis. *Carbohydr. Polym.* **2018**, *180*, 122–127. [[CrossRef](#)]
103. Yu, C.; Zhang, Q.; Zhang, J.; Geng, R.; Tian, W.; Fan, X.; Yao, Y. One-Step in Situ Ball Milling Synthesis of Polymer-Functionalized Few-Layered Boron Nitride and Its Application in High Thermally Conductive Cellulose Composites. *ACS Appl. Nano Mater.* **2018**, *1*, 4875–4883. [[CrossRef](#)]
104. Yang, W.; Xu, J.; Niu, L.; Kang, C.; Ma, B. Effects of high energy ball milling on mechanical and interfacial properties of PBT/nano-Sb<sub>2</sub>O<sub>3</sub> composites. *J. Adhes. Sci. Technol.* **2017**, *32*, 291–301. [[CrossRef](#)]
105. Niu, L.; Xu, J.; Yang, W.; Ma, B.; Kang, C. Crystallization, flame retardancy and mechanical properties of poly(butylene terephthalate)/brominated epoxy/nano-Sb<sub>2</sub>O<sub>3</sub> composites dispersed by high energy ball milling. *J. Macromol. Sci. Part B* **2018**, *57*, 2018.
106. Sharma, N.; Dalvi, A. Mechanical milling assisted synthesis of novel LiTi<sub>2</sub>(PO<sub>4</sub>)<sub>3</sub>-glass-ceramic nanocomposites. *J. Non-Cryst. Solids* **2018**, *483*, 126–133. [[CrossRef](#)]
107. Sabeeh, H.; Aadil, M.; Zulfiqar, S.; Rasheed, A.; Al-Khali, N.F.; Agboola, P.O.; Haider, S.; Warsi, M.F.; Shakir, I. Hydrothermal synthesis of CuS nanochips and their nanohybrids with CNTs for electrochemical energy storage applications. *Ceram. Int.* **2021**, *47*, 13613–13621. [[CrossRef](#)]
108. Pore, O.C.; Fulari, A.V.; Shejwal, R.V.; Fulari, V.I.; Lohar, G.M. Review on recent progress in hydrothermally synthesized MCo<sub>2</sub>O<sub>4</sub>/rGO composite for energy storage devices. *Chem. Eng. J.* **2021**, *426*, 131544. [[CrossRef](#)]
109. Zhu, L.; Liu, N.; Lv, X.; Zhang, Z.; Yu, L.; Li, X. A novel metal-organic framework derived carbon nanoflower with effective electromagnetic microwave absorption and high-performance electrochemical energy storage properties. *Chem. Commun.* **2021**, *57*, 2539–2542. [[CrossRef](#)] [[PubMed](#)]

110. Hou, D.; Guo, Z.; Wang, Y.; Hou, X.; Yi, S.; Zhang, Z.; Hao, S.; Chen, D. Microwave-assisted reconstruction of spent graphite and its enhanced energy-storage performance as LIB anodes. *Surf. Interfaces* **2021**, *24*, 101098. [[CrossRef](#)]
111. Shen, K.; Zhai, S.; Wang, S.; Ru, Q.; Hou, X.; Hui, K.S.; Hui, K.N.; Chen, F. Recent Progress in Binder-Free Electrodes Synthesis for Electrochemical Energy Storage Application. *Batter. Supercaps* **2021**, *4*, 860–880. [[CrossRef](#)]
112. Meng, C.; Das, P.; Shi, X.; Fu, Q.; Müllen, K.; Wu, Z.S. In situ and operando characterizations of 2D materials in electrochemical energy storage devices. *Small Sci.* **2021**, *1*, 2000076. [[CrossRef](#)]
113. Cetinkaya, T.; Tokur, M.; Ozcan, S.; Algul, H.; Uysal, M.; Akbulut, H. Graphene oxide/D-MnO<sub>2</sub> nanocomposite electrodes produced using planetary ball milling for Li-O<sub>2</sub> batteries. *Mater. Today Proc.* **2015**, *2*, 4223–4228. [[CrossRef](#)]
114. Zhang, Z.; Zhao, X.; Li, J. SnSe/carbon nanocomposite synthesized by high energy ball milling as an anode material for sodium-ion and lithium-ion batteries. *Electrochim. Acta* **2015**, *176*, 1296–1301. [[CrossRef](#)]
115. Zhao, H.; Zeng, H.; Wu, Y.; Qi, W.; Zhang, S.; Li, B.; Huang, Y. Facile ball-milled synthesis of SnS<sub>2</sub>-carbon nanocomposites with superior lithium storage. *Prog. Nat. Sci.* **2018**, *28*, 676–682. [[CrossRef](#)]
116. Imamura, H.; Masanari, K.; Kusuhara, M.; Katsumoto, H.; Sumi, T.; Sakata, Y. High hydrogen storage capacity of nanosized magnesium synthesized by high energy ball-milling. *J. Alloys Compd.* **2005**, *386*, 211–216. [[CrossRef](#)]
117. Kahimbi, H.; Hong, S.B.; Yang, M.; Choi, B.G. Simultaneous synthesis of NiO/reduced graphene oxide composites by ball milling using bulk Ni and graphite oxide for supercapacitor applications. *J. Electroanal. Chem.* **2017**, *786*, 14–19. [[CrossRef](#)]
118. Shen, C.; Fang, X.; Ge, M.; Zhang, A.; Liu, Y.; Ma, Y.; Mecklenburg, M.; Nie, X.; Zhou, C. Hierarchical Carbon-Coated Ball-Milled Silicon: Synthesis and Applications in Free-Standing Electrodes and High-Voltage Full Lithium-Ion Batteries. *ACS Nano* **2018**, *12*, 6280–6291. [[CrossRef](#)] [[PubMed](#)]
119. Ji, H.; Hu, S.; Jiang, Z.; Shi, S.; Hou, W.; Yang, G. Directly scalable preparation of sandwiched MoS<sub>2</sub>/graphene nanocomposites via ball-milling with excellent electrochemical energy storage performance. *Electrochim. Acta* **2019**, *299*, 143–151. [[CrossRef](#)]
120. Yi, H.; Lin, L.; Ling, M.; Lv, Z.; Li, R.; Fu, Q.; Zhang, H.; Zheng, Q.; Li, X. Scalable and Economic Synthesis of High-Performance Na<sub>3</sub>V<sub>2</sub>(PO<sub>4</sub>)<sub>2</sub>F<sub>3</sub> by a Solvothermal-Ball-Milling Metho. *ACS Energy Lett.* **2019**, *4*, 1565–1571. [[CrossRef](#)]
121. Wang, X.; Huan, Y.; Zhao, P.; Liu, X.; Wei, T.; Zhang, Q. Optimizing the grain size and grain boundary morphology of (K,Na)NbO<sub>3</sub>-based ceramics: Paving the way for ultrahigh energy storage capacitors. *J. Mater.* **2021**, *7*, 780–789. [[CrossRef](#)]
122. Zhang, C.; Zhitomirsky, I. Influence of High Energy Ball Milling and Dispersant on Capacitive Properties of Fe<sub>2</sub>O<sub>3</sub>-Carbon Nanotube Composites. *J. Compos. Sci.* **2022**, *6*, 177. [[CrossRef](#)]
123. Nguyen, Q.H.; Kim, H.; Kim, I.T.; Choi, W.; Hur, J. Few-layer NbSe<sub>2</sub>@graphene heterostructures as anodes in lithium-ion half- and full-cell batteries. *Chem. Eng. J.* **2020**, *382*, 122981. [[CrossRef](#)]
124. Sun, D.; Ye, D.; Liu, P.; Tang, Y.; Guo, J.; Wang, L.; Wang, H. MoS<sub>2</sub>/Graphene Nanosheets from Commercial Bulky MoS<sub>2</sub> and Graphite as Anode Materials for High Rate Sodium-Ion Batteries. *Adv. Energy Mater.* **2018**, *8*, 1702383. [[CrossRef](#)]
125. Lee, J.J.; Oh, M.Y.; Nahm, K.S. Effect of Ball Milling on Electrocatalytic Activity of Perovskite La<sub>0.6</sub>Sr<sub>0.4</sub>CoO<sub>3-δ</sub> Applied for Lithium Air Battery. *J. Electrochem. Soc.* **2015**, *163*, A244–A250. [[CrossRef](#)]
126. Santhanam, R.; Ghattay, S.; Bobba, R. Effect of ball milling on the electrochemical performance of Li<sub>1.02</sub>Ni<sub>0.4</sub>Co<sub>0.2</sub>Mn<sub>0.4</sub>O<sub>2</sub> cathode synthesized by citric acid-assisted sol-gel process. *Int. J. Electrochem. Sci.* **2010**, *5*, 189–199.
127. Lin, C.; Ouyang, L.; Zhou, C.; Hu, R.; Yang, L.; Yang, X.; Shao, H.; Zhu, M. A novel selenium-phosphorous amorphous composite by plasma assisted ball milling for high-performance rechargeable potassium-ion battery anode. *J. Power Sources* **2019**, *443*, 227276. [[CrossRef](#)]
128. Doppiu, S.; Dauvergne, J.-L.; Serrano, A.; del Barrio, E.P. The Li<sub>2</sub>SO<sub>4</sub>-Na<sub>2</sub>SO<sub>4</sub> System for Thermal Energy Storage. *Materials* **2019**, *12*, 3658. [[CrossRef](#)] [[PubMed](#)]
129. Liu, H.; Hu, R.; Zeng, M.; Liu, J.; Zhu, M. Enhancing the performance of Sn-C nanocomposite as lithium ion anode by discharge plasma assisted milling. *J. Mater. Chem.* **2012**, *22*, 8022–8028. [[CrossRef](#)]
130. Lin, C.; Yang, L.; Ouyang, L.; Liu, J.; Wang, H.; Zhu, M. A new method for few-layer graphene preparation via plasma-assisted ball milling. *J. Alloys Compd.* **2017**, *728*, 578–584. [[CrossRef](#)]
131. Ouyang, L.; Cao, Z.; Wang, H.; Hu, R.; Zhu, M. Application of dielectric barrier discharge plasma-assisted milling in energy storage materials—A review. *J. Alloys Compd.* **2017**, *691*, 422–435. [[CrossRef](#)]
132. Arsalani, N.; Ghadimi, L.S.; Ahadzadeh, I.; Tabrizi, A.G.; Nann, T. Green Synthesized Carbon Quantum Dots/Cobalt Sulfide Nanocomposite as Efficient Electrode Material for Supercapacitors. *Energy Fuels* **2021**, *35*, 9635–9645. [[CrossRef](#)]
133. Liu, X.; Li, Y.; Zeng, L.; Li, X.; Chen, N.; Bai, S.; He, H.; Wang, Q.; Chuhong, Z. A review on mechanochemistry: Approaching advanced energy materials with greener force. *Adv. Mater.* **2022**, 2108327. [[CrossRef](#)]
134. Suryanarayana, C. Mechanical alloying: A critical review. *Mater. Res. Lett.* **2022**, *10*, 619–647. [[CrossRef](#)]
135. El-Eskandarany, M.S.; Al-Hazza, A.; Al-Hajji, L.A.; Ali, N.; Al-Duweesh, A.A.; Banyan, M.; Al-Ajmi, F. Mechanical milling: A superior nanotechnological tool for fabrication of nanocrystalline and nanocomposite materials. *Nanomaterials* **2021**, *11*, 2484. [[CrossRef](#)]